

INSTABILITIES IN A CRITICAL FLOW PROBLEM

by

DAVID LARSEN PORTER

B.S., University of Maryland
(1973)

SUBMITTED IN PARTIAL FULFILLMENT
OF THE REQUIREMENTS FOR THE
DEGREE OF

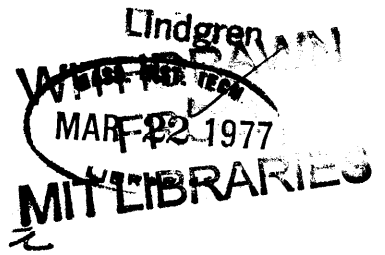
MASTER OF SCIENCE

at the

MASSACHUSETTS INSTITUTE OF TECHNOLOGY

(December 1976)

(12 Feb 1977)



Signature of Author.....
Department of Earth & Planetary Science
December 1976

Certified by.....
John A. Whitehead, Jr. Thesis Supervisor

Accepted by.....
Chairman, Department Earth & Planetary Science

INSTABILITIES IN A CRITICAL FLOW PROBLEM

by

DAVID LARSEN PORTER

Submitted to the Department of Earth and Planetary Science on January 14, 1977 in partial fulfillment of the requirements for the Degree of Master of Science.

ABSTRACT

When a rotating axisymmetric container is emptied through a concentric hole in the bottom, an instability manifested as an azimuthally travelling wave is observed. This wave has a crest that stretches from the inner exit hole to the outer bounding wall and travels in a prograde sense. Experiments demonstrated that this wave had a distinct behaviour as a function of rotation rate of the container, $f/2$, when the exit hole and pumping rates were fixed. The experiments showed that there were four regions of the wave amplitude and wave frequency as functions of f . Two of these regions had a wave frequency that was independent of the rotation rate of the container and the other two had a wave frequency that was dependent upon the rotation rate of the container.

Analytical studies showed that the wave traveled at a speed near the shallow water wave speed and that the solutions to the perturbation equations were singular when the radial velocity was zero or the Froude number unity. Suggested applications of these results are to deep oceanic sill flows, to fluid withdrawal by ocean thermal energy converting plants and to the emptying of fuel tanks on rockets.

Dr. John A. Whitehead, Jr., Thesis Supervisor.

ACKNOWLEDGEMENTS

If I were to list all the people, throughout my life, whom I have had the honor of learning from I would soon bore my reader. For this reason I shall limit my gratitude directly to those involved. Thanks must go to my advisers, Dr. Jack Whitehead, Jr. for his enthusiasm and support and to Dr. Mel Briscoe for his philosophical and enlightening view of science. I would also like to give thanks to my fiancé, Dr. Beverly Bergstorm, for her support through it all.

For technical assistance I thank Mr. Bob Frazel for the hours of help in the laboratory and Mrs. Doris Haight for the large task of typing this paper. I wish to also point out that I was supported by the Ocean Science and Technology Division of the Office of Naval Research, ONR Contract No. N00014-76-C-0197 and by the Oceanographic Section of the National Science Foundation, NSF Grant OCE 72-01562 A03.

In closing I would like to give a special word of thanks to my family; my Father who taught me to question and discover, my Mother who taught me how to finish a task, and to my brothers for their encouragement to me. It is to them, to whom, with respect, this paper is dedicated.

TABLE OF CONTENTS

	<u>Page</u>
ABSTRACT.	2
ACKNOWLEDGEMENTS.	3
LIST OF FIGURES	5
1.0 INTRODUCTION	11
2.0 THE EXPERIMENT	13
2.1 Wave Apparatus.	13
2.2 Lagrangian Tracers.	16
2.3 Stratified Experiment	16
2.4 Experimental Results.	18
2.5 Experiment #1, Small Pump, 3.8 cm hole.	24
2.6 Experiment #2, Small Pump, 4.8 cm hole.	26
2.7 Experiment #3, Large Pump, 3.8 cm hole.	28
2.8 Experiment #4, Large Pump, 4.8 cm hole.	31
2.9 Experimental Conclusions.	33
2.10 Lagrangian Tracer Results	34
2.11 Stratified Experimental Results	41
3.0 THEORY	43
3.1 Steady State Problem.	43
3.2 Dimensional Analysis.	47
3.3 Navier-Stokes Equations	48
3.4 Wave Front.	51
4.0 SUMMARY.	57
APPENDIX A.	60
APPENDIX B.	62
REFERENCES.	67
BIOGRAPHY	68

FIGURE CAPTIONS

<u>No.</u>	<u>Title</u>	<u>Page</u>
2.1	<p>A cutaway schematic of the apparatus used for the investigation of the wave. The letters refer to the following:</p> <p style="margin-left: 40px;">H the water P the pump C the catch basin Sl the inner screen wall G the gravel filler S the shaft of the table O the loop of feeder hose R the exit hole</p> <p>The table rotated at frequency $f/2$. Note the shape of the free surface of the fluid in the tank.</p>	14
2.2	<p>A schematic of the setup using the strobe light to obtain pictures of particle paths. The letters refer to the following:</p> <p style="margin-left: 40px;">T the tank L the strobe light CN the camera H the water S the shaft P the pump</p> <p>The tank rotated at frequency $f/2$.</p>	14
2.3	<p>This is the apparatus used for experiments in the rotating stratified flows. The top layer, 1, was placed in the tank and then spun up to frequency $f/2$. The second and third layers were then put in while the tank was rotating, through the use of the funnel, F. The denser fluid would come up through the gravel bed, G, thereby being forced into solid body rotation with the table. The water was then withdrawn at a rate of $8 \text{ cm}^3/\text{sec}$ into a reservoir, R, by the pipe, W. The entire apparatus was mounted on a one meter turntable. The densities in the layers are:</p> <p style="margin-left: 40px;">1. $\rho = 0.9975 \text{ gm/cm}^3$ 2. $\rho = 1.0053 \text{ gm/cm}^3$ 3. $\rho = 1.0125 \text{ gm/cm}^3$</p>	17

<u>No.</u>	<u>Title</u>	<u>Page</u>
2.4	This shows a typical result of an experimental run. This was for the large pump ($640 \text{ cm}^3/\text{sec}$) and a 4.8 cm radius exit hole. The height of the fluid is measured near the diffuser and exhibits an f^2 behaviour. It appears that there is an onset of the wave at approximately $f = 1$ rad/sec, though it will be shown in Figure 11 that a wave actually appears earlier but is hidden here due to instrument noise. The wave then persists throughout the frequency range of this experiment though it does change character at approximately $f = 2$ rad/sec and $f = 2.6$ rad/sec. The frequency of the table was slowly increased every 15 seconds from $f = 0$ rad/sec to $f = 4$ rad/sec over a span of 35 minutes. The rotation rate was then decreased back to zero and though the same pattern emerged, it appears that the cutoff is at the frequency of approximately $f = 0.8$ rad/sec. The numbers 1-5 on the graph will be explained in the following figure.	20
2.5	Plots of pressure versus time at values of f corresponding to the indicated places in Figure 5. The tick marks below each curve were recorded directly from a switch on the turntable and correspond to one table revolution. The hole was at $r = 4.8$ cm, the diffuser at $r_1 = 15.0$ cm and the probe at $r_2 = 14$ cm. The time scale at the bottom is in seconds, and the height of the wave diminishes as can be seen from the scaling on the right. Important features to note are that the wave is not locked to the rotation of the table and that the shape of the wave changes dramatically with frequency. The wave profiles in case 1 are very much like a bore whereas in 3 they are tooth-like. The jagged small scale behaviour in 4 and 5 is due mainly to instrument noise. Later experiments in the range of 4 and 5 showed almost an infinitesimal sinusoid.	22

<u>No.</u>	<u>Title</u>	<u>Page</u>
2.6- 2.9	A series of experiments with different size pumps and exit holes were made. The pressure measurements were recorded along with table rotations on a strip chart. Frequencies and amplitudes of the wave were measured from the graph and plotted against the rotation rate of the table. The frequency of the waves were corrected for Doppler shifting by the formula $v_w = v_m - v(r)/r$ where v_m is the measured frequency of the wave, v_w is the actual frequency of the wave and $v(r)$ is the steady state azimuthal velocity obtained by Whitehead and Porter (1976). Transitions in frequency are often paralleled by transitions in amplitude. The frequency of the wave and the amplitude are plotted on the ordinate and the rotation rate of the table is plotted on the abscissa.	25-32
2.6	This was the case of the small pump (400 cm ³ /sec) and hole of radius 3.81 cm. Note that the frequency of the wave remains almost constant at $v = 3.3$ rad/sec until $f = 1.1$ rad/sec. Here the wave dies in amplitude before coming back as a finite amplitude wave with a frequency which behaves as $f \cdot 59$. This frequency behaviour persists even as the amplitude decreases once more.	25
2.7	As in the previous figure the small pump was used, but the hole was increased to 4.8 cm. The amplitude roughly remains constant over the entire frequency range considered. The wave frequency is constant at $v = 3.4$ rad/sec until the break which occurs at $f = 1.72$ rad/sec and thereafter it exhibits a slope proportional to $f \cdot 59$.	27
2.8	The large pump (640 cm ³ /sec) and 3.81 cm radius hole were used in this experimental run. The wave was of finite amplitude and equal in magnitude to the water depth over the region $f = 0.55$ rad/sec to $f = 1.2$ rad/sec. At $f = 1.34$ rad/sec there is a transition in amplitude to a regime that strongly resembles	

<u>No.</u>	<u>Title</u>	<u>Page</u>
	the beating of two frequencies. The "beating" region is marked on the graph by the shaded region. The top bounding line on that region was the maximum amplitude of the wave and the bottom boundary line was the minimum amplitude of the wave. This region was not present in the previous figures. Then at $f = 2$ rad/sec the finite amplitude wave returns and then begins to decrease as the rotation rate of the table is increased. Even though the amplitude goes through three different transitions the wave frequency still exhibits the type of behaviour observed in the previous figures. It remains roughly constant at $\nu = 4$ rad/sec and then at $f = 2.01$ rad/sec (the same point as the "beating" occurred) the wave frequency begins to increase at a rate of $f \cdot 52$.	29
2.9	The most unusual of all results occurred for the large pump ($640 \text{ cm}^3/\text{sec}$) and hole radius of 4.8 cm. It has a region called the "micro-wave" range where the amplitude was just measurable. This had a high frequency of 6.3 rad/sec and was stable. At $f = 1$ rad/sec a finite amplitude wave is set on and the frequency of the wave is reduced to 4.3 rad/sec. At $f = 2.05$ rad/sec there is again the "beating" effect and the wave begins to die away until at approximately $f = 2.88$ rad/sec there is a large finite amplitude wave with a frequency dependence of $f \cdot 47$.	32
2.10- 2.11	These are made from the strobe light photographs of particle positions in the wave tank. All cases are for the large pump ($640 \text{ cm}^3/\text{sec}$) and a hole radius of 4.8 cm. It was impossible from the photographs to ascertain the position of the wave crest at any given time. The circle is the exit hole. The frequency in the right hand bottom corner corresponds to the table rotation and corresponds to a wave frequency and amplitude which may be obtained from Figure 2.9.	36-37

<u>No.</u>	<u>Title</u>	<u>Page</u>
2.10	The three separate tracks demonstrate that the flow is by no means steady. Some flows exhibit the spiraling predicted by theory while others behave as if the flow were not rotating at all. The time between dots is .025 sec.	36
2.11	This figure is a remarkable plot in that there exists a flow shown by the spiraling pattern where the fluid velocity has a radial component outward. The time between dots is .025 sec.	37
2.12- 2.14	This series of diagrams is made using the same parameters as in the previous two photographs. However, instead of a strobe light a 16 mm movie of the wave was made. The time between dots is .05 seconds.	38-40
2.12	There was a bore present in this case and the flow was sometimes radially in and at other times in the form of a spiral depending upon the position of the wave.	38
2.13	This wave also exhibits, as did Figure 13, the flow reversal.	
2.14	This shows the flow at high rotation rate when the wave was very small in amplitude and most effects were due just to that explained by steady state theory.	40
2.15	This is a photograph of the stratified experiment. There exists on the outside of the cone of fluid a rather fuzzy coating (arrow) that rotated rapidly in the prograde sense. It is suggested that this might be the stratified case for the instability.	42
3.1	Experimental observations of the height at some rotation rate f minus the height for the same pumping rate at $f = 0$ times a correction factor	

$$C = 8g r_0^2 / \left(1 - \frac{r_0^2}{r_2^2}\right) (r_1^4) .$$

<u>No.</u>	<u>Title</u>	<u>Page</u>
3.1 (Contd.)	In all runs the radius of the hole $r_0 = 4.8$ cm, radius of the diffuser $r_1 = 15.0$ cm; (o) - $Q = 136$ cm ³ /sec, $r_2 = 13.8$ cm where r_2 is radius of the height measuring probe; (•) - $Q = 533$ cm ³ /sec, $r_2 = 13.3$ cm. The interval between the two W's exhibited a traveling wave on the flow for $Q = 533$ cm ³ /sec. The six circles in the upper right may have been influenced by an Ekman-layer flux as discussed in the text.	46
3.2	This is a Fourier decomposition of the waves as exemplified in curves 1 and 3 of Figure 2.5. Line B corresponds to a wave frequency of 4.64 rad/sec and C to a wave of frequency of 5.20 rad/sec. Both have been normalized by their means so that the amplitude, A , is 1 at $f = 0$ rad/sec. Though one is a shorter record than the other, the salient features are evident. The amplitude of the sawtooth wave is higher in the lower frequencies than that of the bore whereas at higher frequencies the bore has a higher amplitude thus stressing the nonlinear effects. From $f = 1$ rad/sec to $f = 2$ rad/sec the fall off in the B-type wave is one-half whereas it is one-fifth for the C-type.	54
3.3	The figure shows the exit hole centered about the origin O and the wave crest extending out to the radius r_1 . The radial and azimuthal vectors are \hat{r} and $\hat{\theta}$, respectively. \hat{n} is the normal to the wave crest. $\vec{u} = u(r)$, the radial velocity and $\vec{v} = v(r) - vr$, the azimuthal velocity of water in the wave frame of reference.	55
3.4	This shows the radial distance of the wave crest, R , as a function of $-\theta$. The solid line D is the wave crest measured from the experiment where $Q = 640$ cm ³ /sec, $r_0 = 4.8$ cm and $f = 1.5$ rad/sec. The dotted line, T, is the theoretical calculation. The value went complex at $R = 6$ cm.	56

1.0 INTRODUCTION

Under certain conditions when a fluid is spun up in a cylindrical container and emptied through a hole centered in the container's bottom, an instability in the flow occurs in the form of an azimuthally travelling wave. The observation of this instability was made during an investigation of the steady state critical withdrawal of a fluid from a rotating cylinder. In this investigation Whitehead and Porter (1976) studied the inviscid, vertically integrated Navier-Stokes equations and were able to obtain a theoretical prediction of the way in which the fluid emptied out of the container. They then built a laboratory experiment analogous to the steady state emptying problem and while making measurements to test the theory, observed an instability manifested as this azimuthally travelling wave. The crest of the wave stretched from the exit hole to the outside wall of the container and propagated in the prograde sense. The wave had a frequency approximately five times that of the rotating container and its amplitude varied for different parameters from an infinitesimal height to heights equal to the fluid depth.

The results of the investigation of this instability have interesting applications outside the specific field of rotating critical flows. For example, it is possible that the mechanism that feeds this instability is also at play in the deep sill flows between the major ocean basins. Some suggestive evidence for this is from current meter data taken at the Windward Passage which shows strong bursts in velocity over periods of days. These bursts

are intermittently added to a steady mean flow that exists at the sill (Stalcup, personal communication). Another possible oceanic application is in the operation of the ocean thermal energy converting power plants (OTEC) (Anderson and Anderson 1966, Zener 1973) which will withdraw large quantities of water from below the thermocline. This not only gives rise to the question of how important the earth's rotation will be in the withdrawal of the water but also to the question of whether or not this instability will affect the plant's function. One last application from a rather different field of study is the emptying of fuel tanks on rockets. If the fluid has a slight spin as it is being emptied it may be that the wave can be onset and thereby provide an unfavorable torque on the vehicle.

The following sections of this paper are concerned with the details of both the experimental and theoretical results. The experimental results in Section II entail both a detailed description of the apparatus used and the results of the experiments performed. Section III is the theoretical section and begins with a review of the steady state solution for critical withdrawal by Whitehead and Porter. Attempts are made using dimensional analysis, kinematic conditions and the full, time-dependent Navier-Stokes equations to obtain the controlling parameters of the flow. The last part, Section IV, is a summary with suggested applications of the results to fluid withdrawal problems.

2.0 THE EXPERIMENT

2.1 Wave Apparatus

The apparatus allowed a steady uniform flow from the outside wall of a right circular cylinder to a concentric inner exit hole to be maintained while the rotation rate of the apparatus was varied (see figure 2.1). The right circular tank was constructed of 1/8" plexiglass. The height and outside radius of the tank were 17 cm and 20 cm, respectively. The top of the tank was open and the bottom of the tank was flat. A concentric hole 4.8 cm in radius was cut in the bottom.

A diffuser which formed the inner wall of the apparatus allowed the fluid to flow uniformly in from the outside wall. The diffuser had a window screen wall that stood 15 cm high and had a radius of 15 cm. This wall was positioned concentrically in the tank leaving a space between the outer plexiglass wall and the inner screen wall. The interstitial space was filled with gravel of mean diameter 1 cm. Imbedded in this gravel was a loop of hose, closed at one end and connected to rubber tubing at the other end. The tubing was connected to a submersible pump. The hose of outside diameter 2.5 cm ran around the circumference of the screen wall and had holes of diameter .25 cm drilled in it every 2.4 cm.

The entire apparatus described above was mounted over a catch basin that contained the submersible pump as well as the fluid. When the pump was turned on the fluid was drawn up and forced through the tubing, into the loop of hose imbedded in

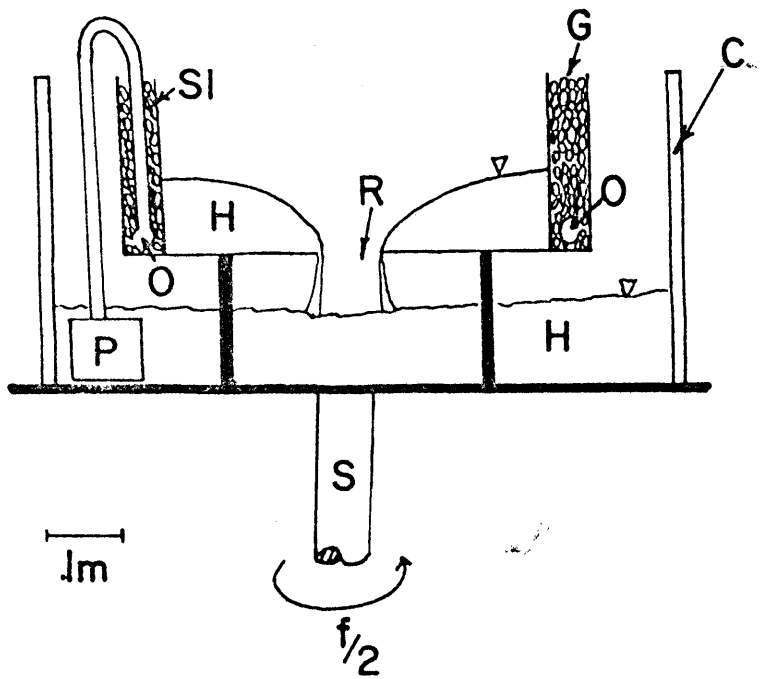


Figure 2.1

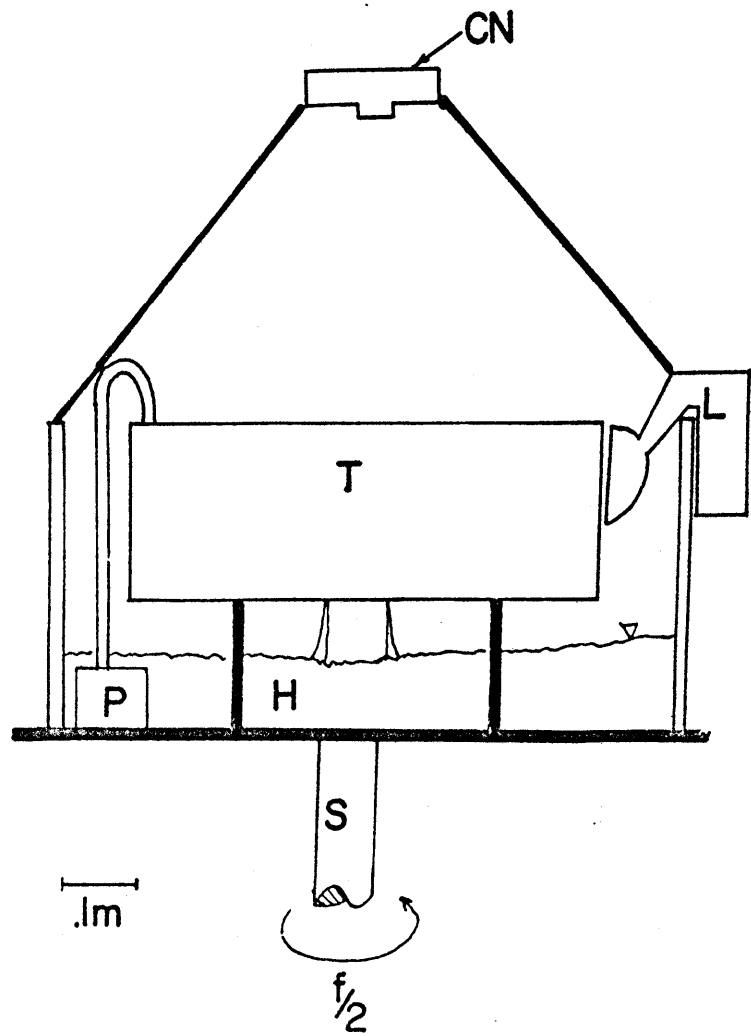


Figure 2.2

the gravel. The fluid flowed out the holes that were drilled in the hose, into the porous medium, and out the screen wall. An axisymmetric flow was obtained as the fluid entered uniformly with a velocity vector normal to the screen wall. The radially inward flow was terminated at the exit hole where the fluid fell through to the catch basin where it began its journey once more.

The variable parameters of the experiment were the rotation rate, the exit hole size and the pumping rate. The rotation rate was varied by mounting the entire apparatus on a variable speed turntable. A slowly revolving d.c. motor was connected to the table's transmission allowing the rotation rate of the table to be changed slowly and continuously. A typical acceleration was from $f = 0$ rad/sec to $f = 4$ rad/sec in a one and one-half hour period. The d.c. motor could be reversed to run the same experiment with the rotation rate decreasing. The exit hole size was varied by constructing false bottom inserts with holes 1.27 cm, 2.54 cm, 3.81 cm, and 4.8 cm in radius. The pumping rate was varied by the use of two different pumps with flow rates of $640 \text{ cm}^3/\text{sec}$ and $400 \text{ cm}^3/\text{sec}$. (See Appendix A for a discussion of errors in measurements.)

The height of the fluid measured at a point and the table revolution were simultaneously recorded on a strip chart recorder. The measuring system for the fluid height was a "tyco" LP pressure transducer, linear to 1% over its 1 psi pressure range. The transducer was connected by a .2 cm outside diameter stainless steel tube, 23 cm in length, to the tank's

bottom. The signal from the transducer was recorded on a two channel strip chart recorder. In addition there was a magnetic switch on the turntable that recorded each table revolution on the other channel of the recorder. The table frequency, wave frequency, wave amplitude and fluid depth were calculated from the information recorded on the strip chart.

2.2 Lagrangian Tracers

A variation on the apparatus described in Section 2.1 allowed the fluid motion to be observed by use of Lagrangian tracers (Figure 2.2). A camera mounted over the apparatus in the rotating frame of reference was used to obtain pictures of the position of small pieces of paper. The shutter of the camera was left open and a strobe light mounted on the side of the apparatus was turned on. Thus a time lapse photograph of particle position was made. This experiment used only the large pump and the largest exit hole. No wave front information was obtained. The particle paths for a few of the runs are plotted in figures 2.10 and 2.11.

2.3 Stratified Experiment

A different experiment was run that was an attempt at the stratified analogue of the experiment described in Section 2.1. The apparatus used in this experiment was a plexiglass tank that stood 31 cm high and had a square bottom measuring 38 cm on the side (see figure 2.3). The bottom of the tank had a gravel bed with a hose imbedded in it. The hose ran up along the corner of the tank and then to a funnel supported dead center

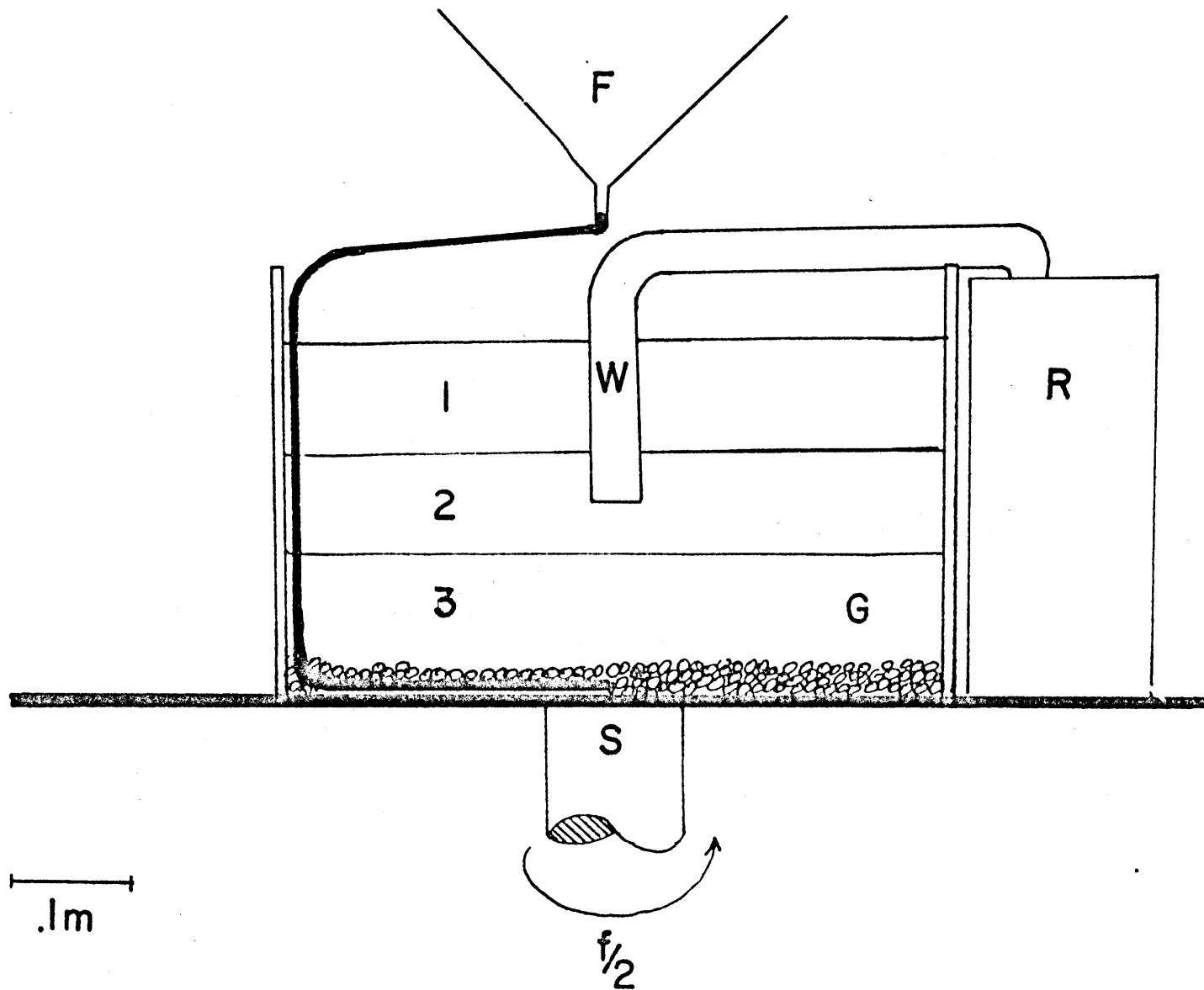


Figure 2.3

over the tank. The lightest fluid of density $.9975 \text{ gm/cm}^3$ was then poured into the tank and spun up. A second fluid of salt-induced density 1.0053 gm/cm^3 was introduced through the rock bed at the bottom by pouring the fluid into the funnel while the apparatus was in rotation. This allowed the fluid to come into the tank in solid body rotation. A third fluid of density 1.0125 gm/cm^3 was introduced last. A withdrawal pipe of outside radius 1.27 cm was inserted in the fluid along the axis of rotation and it extended down to the middle layer. A siphon was started that emptied the fluid out at a rate of $8 \text{ cm}^3/\text{sec}$. A camera mounted on a tripod in the lab frame recorded the fluid withdrawal. A result is shown in figure 2.15.

2.4 Experimental Results

An experimental run consisted of slowly increasing the rotation rate of the table while keeping all other parameters constant. Having fixed the hole size and pumping rate, the recording devices and the motor drive on the transmission were activated. Once the wave was onset it was possible to determine the frequency of the wave, ν , and the frequency of the table $f/2$ from the record made. The wave had a crest stretching from the inner hole to the outer wall and traveled in a prograde sense. The amplitude of the wave and the frequency of the wave were then plotted as functions of the table rotation f in figures 2.6-2.9.

Figure 2.4 represents a typical result from the strip chart recorder. The figure shows the fluid height plotted on the ordinate of the graph with f plotted on the abscissa of the graph and the actual time into the experiment on the axis at the top. The noise in this experiment was approximately .1 cm. The speed of the chart paper was slow such that the actual oscillations of the wave are not discernible, but their crests and troughs are easily demarked. This experiment had as parameters the large pump ($640 \text{ cm}^3/\text{sec}$) and large hole (4.8 cm). One of the first features to be observed is the mean trend which follows the curve f^2 exactly. This f^2 behaviour is predicted by the steady state theory.

Superimposed on the mean height is the prominent wave. As f increases from $f = 0 \text{ rad/sec}$ to $f = 1 \text{ rad/sec}$ there is no apparent wave. After $f = 1 \text{ rad/sec}$ there is the onset of a finite amplitude wave with the amplitude at times equal to the water depth. At $f = 2 \text{ rad/sec}$ there is an onset of a different type of wave. This wave is somewhat hidden in this graph, but has the characteristic form for the beating between waves of two different frequencies. The finite amplitude wave is attained again at the frequency of $f = 2.25 \text{ rad/sec}$ and lasts until $f = 2.6 \text{ rad/sec}$ where the finite amplitude dies away and just a small amplitude wave remains. This small amplitude wave remains until the experiment is terminated at $f = 4 \text{ rad/sec}$. Upon decreasing the table rotation rate the same results are obtained with the exception that the points where the transitions occur are at lower frequencies and not as sharp as on the up trace.

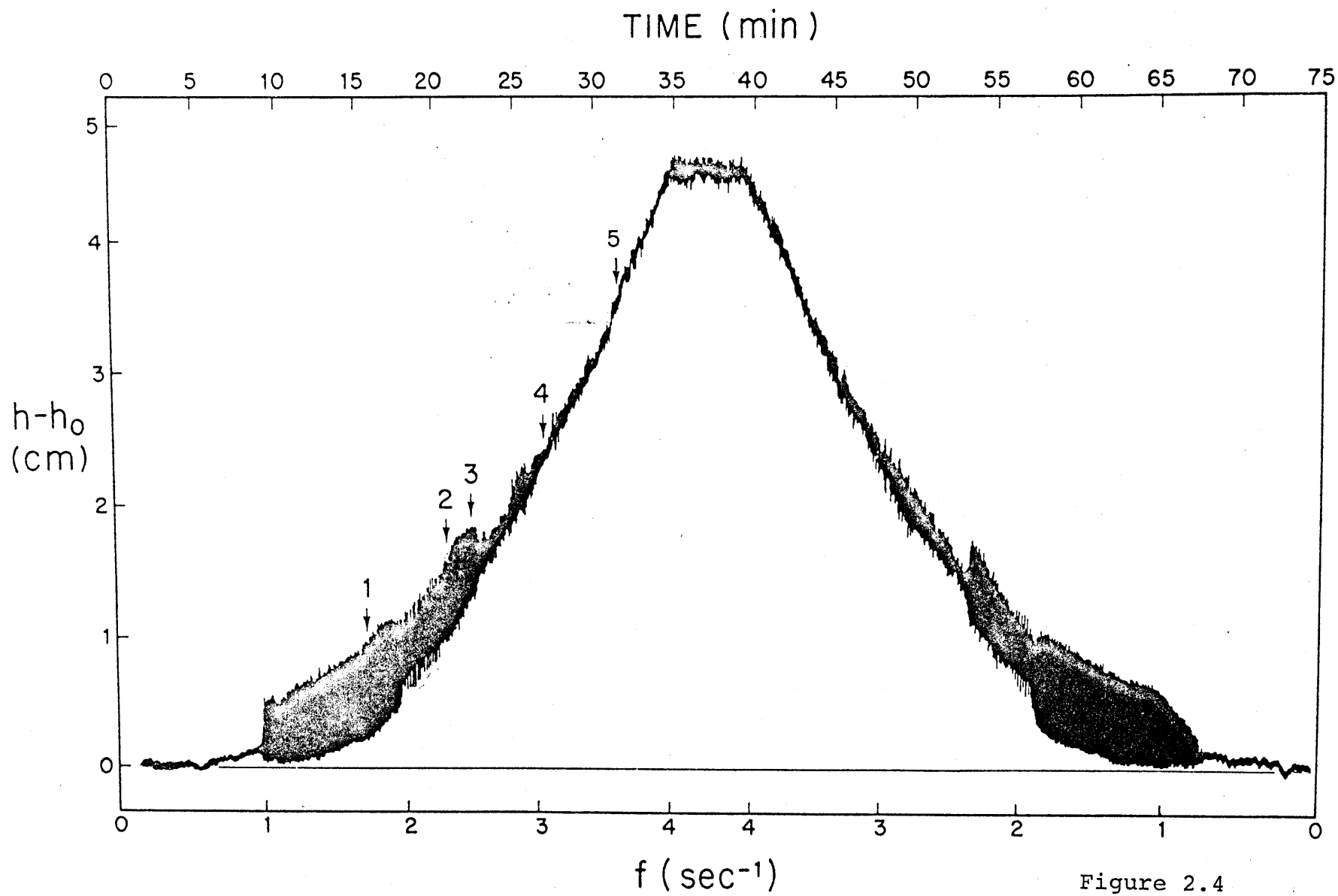


Figure 2.4

The transition in wave frequency paralleled the transitions in amplitude. For this case the wave frequency remained constant from $f = 1$ to $f = 2$ rad/sec and increased as approximately the square root of f after $f = 2$ rad/sec. The important features to be gleaned from the above example is (1) the range in f where the wave's frequency remained constant, (2) that there was a transition in which the wave frequency was a function of f , and (3) that this transition in frequency was paralleled by a transition in amplitude.

The wave profile changed its character as a function of table frequency also. Figure 2.5 shows that at low frequencies (wave 1, figure 2.5), when the wave was of finite amplitude, the wave profile had the shape of a bore with a sharp leading edge and a sloping back (the numbers refer to numbers marked on figure 2.4). As the frequency of the table was increased to $f = 2.4$ rad/sec the wave labeled 3 in the graph became the classical triangular type. As the frequency was increased even more the amplitude of the wave became almost hidden in the noise of the instrument as exemplified by 5 in figure 2.5. From this figure one can gain an understanding of the type and shape of the waves that were appearing.

In summary, as the frequency of the table was slowly increased there appeared a number of transitions both in amplitude and in wave frequency of the instability. As f was increased the amplitude went from zero to a finite value, to a form resembling the beating between two waves, to a finite value again

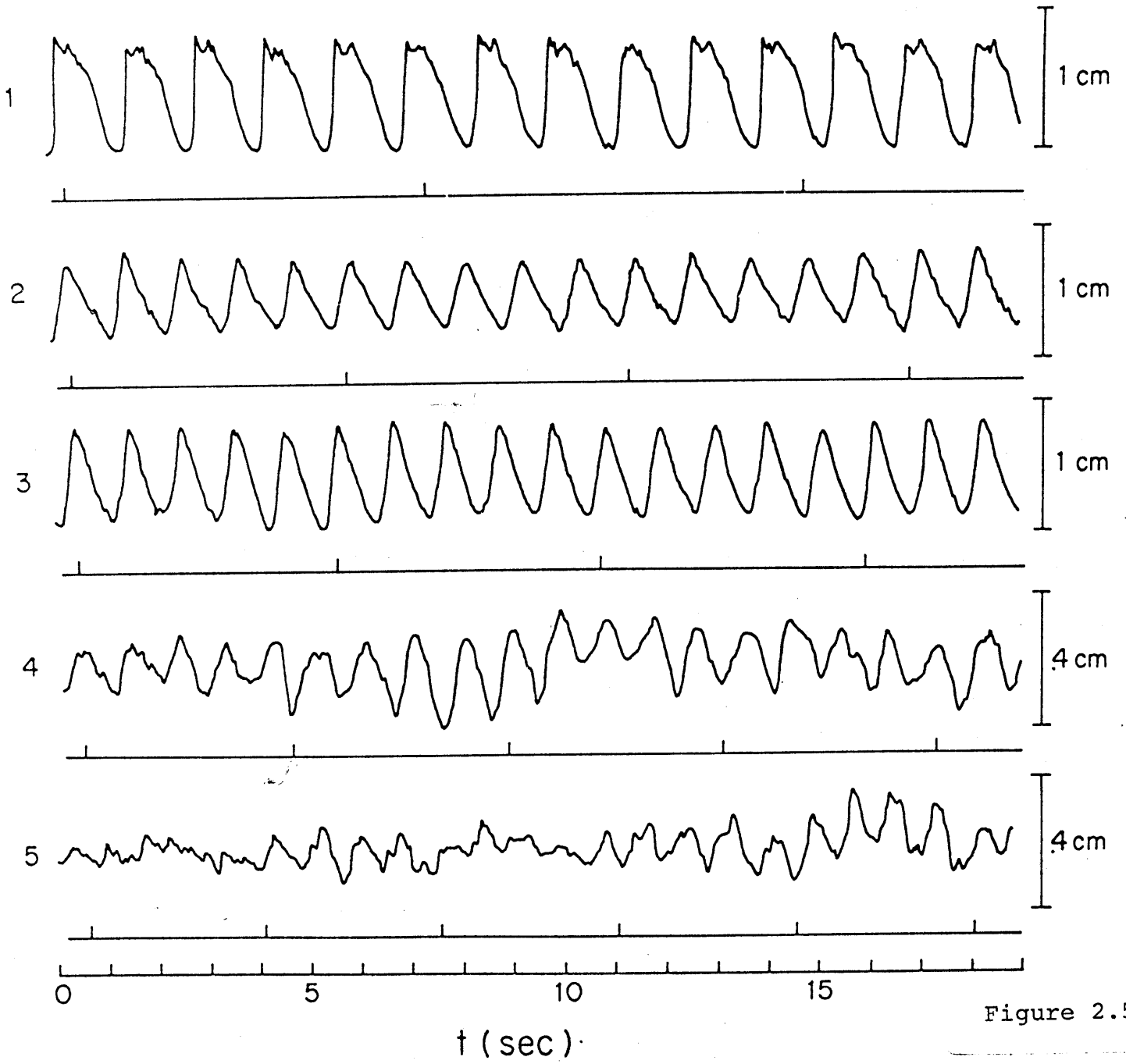


Figure 2.5

and then down to a very small value. During these transitions in amplitude there were sometimes concurrent transitions in frequency. The wave frequency was independent of table rotation for a certain range in f and it increased as approximately the square root of f over a different range in f . It was hard to tell if all amplitude transitions were accompanied by an actual transition in wave frequency.

The table frequency, wave frequency and amplitude of the wave were all computed from the recording made by the strip chart recorder. The calculations of the amplitude of the wave and the rotational frequency of the table are straightforward. The calculation of wave frequency required a correction for Doppler shifting. The probe used to measure the wave was positioned inside of the wire wall where there was a v component of velocity. Hence, the equation for the Doppler correction was

$$\nu = \nu_m - \frac{v(r)}{r} \quad (\text{See Appendix B for comparison of actual } \nu \text{ and } \nu_m.) \quad (2.a)$$

Where ν is the actual wave frequency, ν_m is the measured wave frequency, and $v(r)$ is the steady state azimuthal velocity as is computed in Section 3.1, and r is the radius measured from the axis of rotation. The amplitude and wave frequencies were then plotted up as functions of the table rotation rate f . Calculations showed that the results were the same, independent of whether or not the rotation rate was increasing or decreasing, therefore only the up trace was used in the computations.

Four experiments were run with two different exit holes and two different pumping rates. These are discussed in the

following four sections with a review of the amplitude response as a function of f and then a review of the wave frequency response as a function of f . A conclusion with all salient facts is then presented in closing each discussion of the experiment.

2.5 Experiment #1 Small Pump, 3.8 cm hole

In the first experiment with the small pump ($400 \text{ cm}^3/\text{sec}$) and 3.8 cm hole there were two transitions in amplitude that had corresponding transitions in wave frequency (see figure 2.6). The signal jumped to a large amplitude wave at $f = .44 \text{ rad/sec}$. This large amplitude wave, which was more of a large triangular type wave than a bore, persisted until $f = 1.2 \text{ rad/sec}$ where the amplitude began to decrease to almost zero. At $f = 1.5 \text{ rad/sec}$ the large amplitude wave returns and remains strong until $f = 2.2 \text{ rad/sec}$ where its amplitude slowly decreases as a function of f until $f = 4 \text{ rad/sec}$ when the experiment was stopped. It is important to note that no apparent "beating" took place in the course of the experiment and that the transition in amplitude occurred at $f = 1.4 \text{ rad/sec}$.

The transitions in frequency of the wave mirrored the transitions of the amplitude. The wave frequency was independent of table rotation from the range $f = .44 \text{ rad/sec}$ to $f = 1.38 \text{ rad/sec}$. The frequency, ν equalled 3.3 rad/sec . At the same point at which the transition occurred in amplitude a transition occurred in frequency. At $f = 1.38 \text{ rad/sec}$ the wave frequency jumped to approximately $\nu = 5 \text{ rad/sec}$ and afterwards steadily increased as a function of $f^{.59}$. This slope was determined by a least squares fit to the data after the transition point.

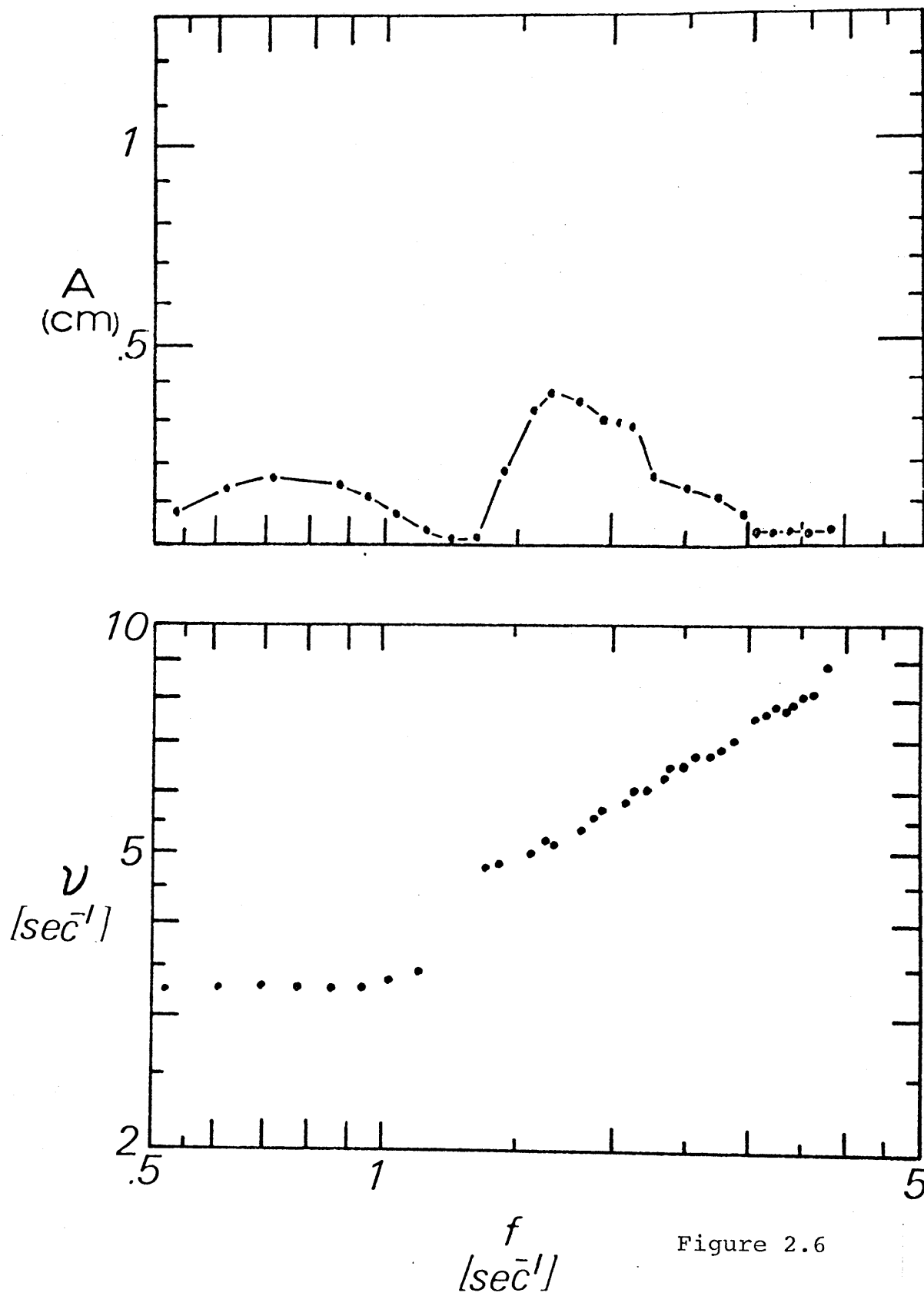


Figure 2.6

The two most important results from this experiment were that the transitions in amplitude were accompanied by transitions in frequency and that the wave frequency had an entirely different behaviour on each side of the transition. The wave frequency was independent of the table rotation until $f = 1.38$ rad/sec whereafter the wave frequency increased as $f^{.59}$. An important negative result was that of the absence of "beating."

2.6 Experiment #2 Small Pump, 4.8 cm hole

The second experiment, that of the small pump ($400 \text{ cm}^3/\text{sec}$) and large hole (4.8 cm) was important in that no transitions occurred in amplitude even though transitions appeared in frequency (see figure 2.7). The wave was onset at $f = .73$ rad/sec and remained at an amplitude of about .1 cm until the termination of the experiment at $f = 4.3$ rad/sec. There were no apparent transitions, finite amplitude responses, or "beating" throughout the entire range of table rotation rates.

The frequency of the instability for this experiment had a behaviour similar to that of the first experiment. The wave frequency of the instability was independent of the table frequency for the range $f = .73$ rad/sec to $f = 1.7$ rad/sec at a value of $\nu = 3.4$ rad/sec. From a frequency of 1.7 rad/sec until the termination of the experiment the wave frequency increased as $f^{.59}$.

The two most important results from this experiment were that there were no apparent transitions in amplitude and that the response and behaviour in frequency were very similar to

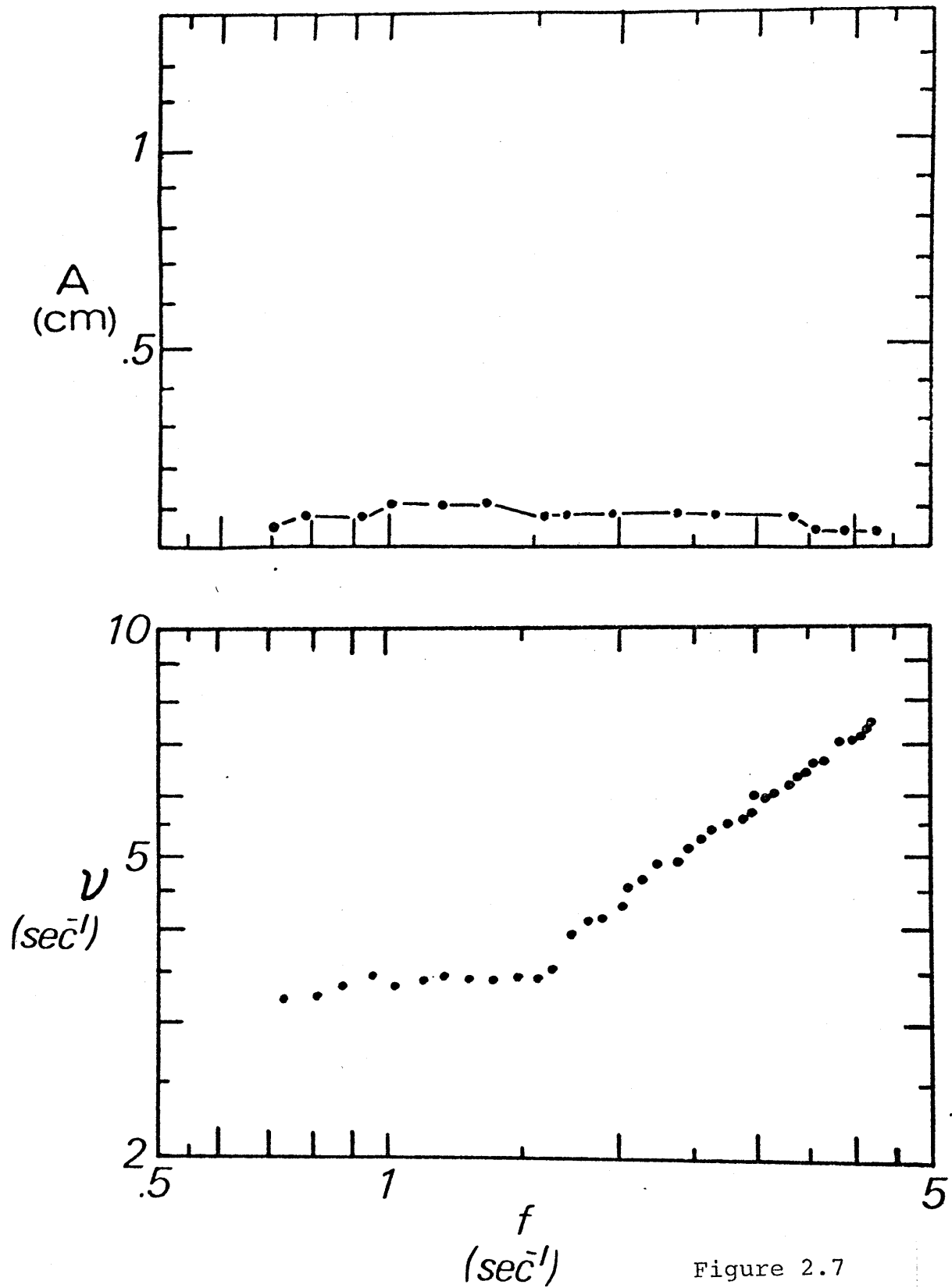


Figure 2.7

that of the first experiment. The wave attained an amplitude of approximately .1 cm and showed a transition in frequency at 1.7 rad/sec. A constant frequency preceded the transition and an f dependent frequency followed the transition.

2.7 Experiment #3 Large Pump, 3.81 cm hole

The amplitude response of this experiment with the large pump ($640 \text{ cm}^3/\text{sec}$) and 3.81 cm hole goes through three different transitions (see figure 2.8). At a frequency of $f = .46 \text{ rad/sec}$ there is a large finite amplitude bore that travels in the pro-grade sense. This bore remains at an amplitude of .6 cm until $f = 1.33 \text{ rad/sec}$. It is at this frequency of 1.33 rad/sec where the wave goes into what looks like a beating between two waves of different frequency. What causes this beating? Could it be that there is a small tide, due to the table not being perfectly level, that is being added to the ambient wave and therefore giving rise to this beating? If we consider the process of adding two waves of equal amplitude together linearly by the following formula

$$\cos \omega_1 t + \cos \omega_2 t = 2 \cos \bar{\omega} t \cos \Delta \omega t$$

with

$$\bar{\omega} = \frac{\omega_1 + \omega_2}{2}, \quad \Delta \omega = \frac{\omega_1 - \omega_2}{2}, \quad (2.b)$$

then the classical result of beating between two frequencies is obtained. Let $\omega_2 = .67 \text{ rad/sec}$ be the frequency of the tide and $\omega_1 = 4.2 \text{ rad/sec}$ be the frequency of the wave. These values give for $\bar{\omega}$ and $\Delta \omega$ values of 2.45 rad/sec and 1.76 rad/sec, respectively.

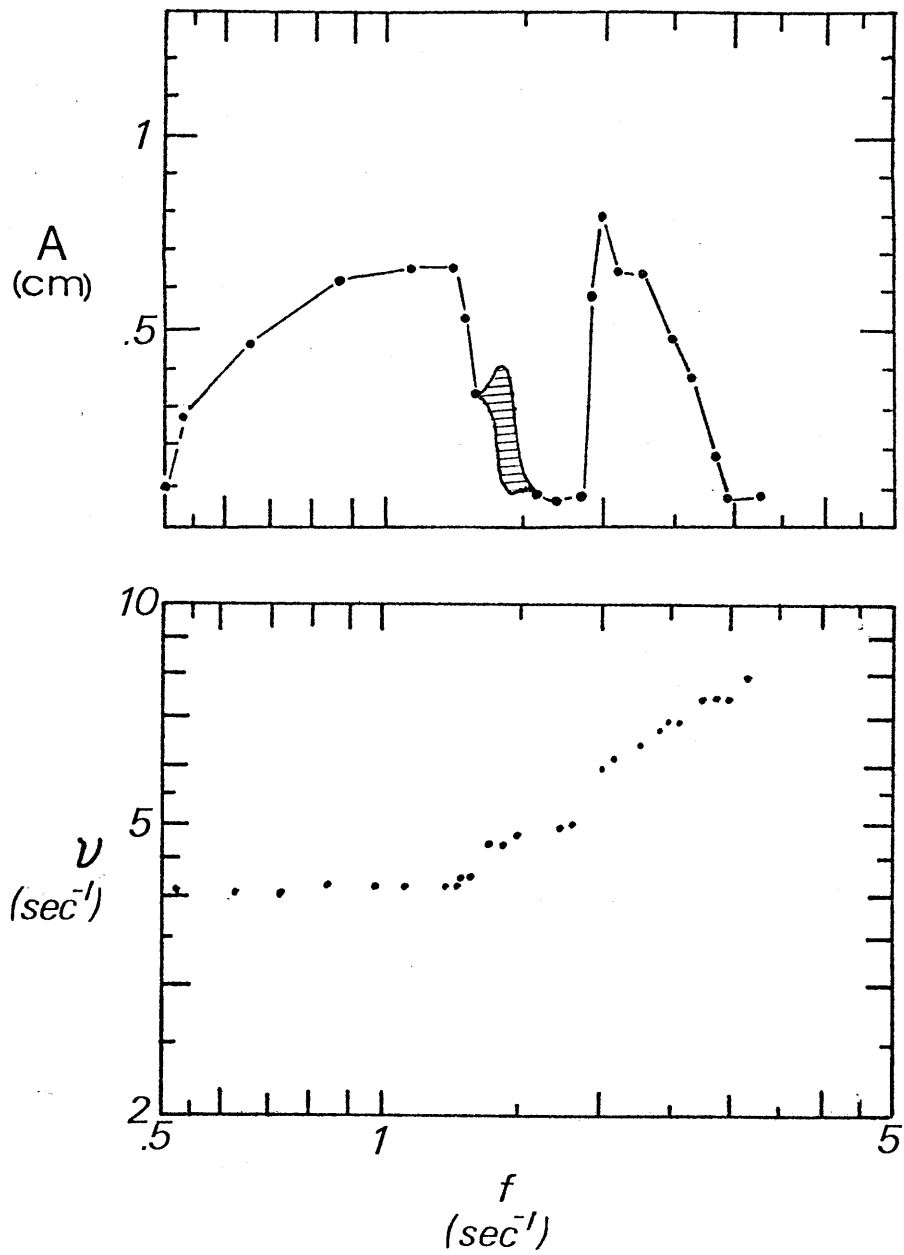


Figure 2.8

The actual measured values are $\Delta\omega = 4.6$ rad/sec and $\bar{\omega} = .62$ rad/sec. Thus it appears that what looks like "beating" between two waves is not that at all but must be some response of the instability itself. After this "beating" event the amplitude begins to die away as f is increased. At $f = 2.01$ rad/sec the finite amplitude wave returns and reaches an amplitude of .7 cm. For values greater than $f = 2.01$ rad/sec the wave's amplitude slowly decreases as f increases until the experiment is terminated.

In the previous experiment some of the transitions in amplitude were paralleled by transitions in frequency and it appears that this same result may be ascertained from the three transitions that occur in this experiment. Using the amplitude as a guide, the frequency range may be broken into three regions. Those regions are (1) $f = .46$ rad/sec to $f = 1.33$ rad/sec, (2) $f = 1.33$ rad/sec to $f = 2.01$ rad/sec, and (3) $f = 2.01$ rad/sec to 3.4 rad/sec when the experiment was stopped. In the first region the wave had a constant frequency of $\nu = 4.2$ rad/sec. In the second region (where the "beating" occurred) the frequency of the wave behaved as $f^{.42}$. And in the third region the wave had an $f^{.52}$ dependence in frequency. It is hard to actually observe this break in slope of the frequency dependence. If the region from $f = 1.33$ rad/sec to $f = 3.4$ rad/sec was used to compute the f dependence of wave frequency, then a dependence of $f^{.54}$ would be found. Therefore, it is hard to state explicitly that there is or is not a transition in frequency between the "beat" behaviour and the finite amplitude behaviour.

There appears to be good evidence for two transitions and weaker evidence for a third transition in this experiment. As in previous experiments there is a region where v is independent of the rotation rate of the table and also a region where the wave is of large amplitude and increasing in frequency as approximately the square root of f . It may be that the "beating" has a frequency behaviour different from the behaviour when f is large though that remains to be proved. The "beating" that occurred in this experiment was shown to be a property of the instability rather than a beating between two waves of different frequencies.

2.8 Experiment #3 Large Pump, 4.8 cm hole

The experiment performed with the large pump ($640 \text{ cm}^3/\text{sec}$) and large hole (4.8 cm) had an amplitude response which not only showed results similar to the previous experiment but an entirely new region altogether (see figure 2.9). This new region is given the name "microwave" region, not due to its wavelength but rather to its amplitude. Its amplitude is approximately .02 cm and is constant at this value over the range from $f = .56 \text{ rad/sec}$ to $f = 1.06 \text{ rad/sec}$. At $f = 1.06 \text{ rad/sec}$ a finite amplitude bore is onset. This bore persists until $f = 2.09 \text{ rad/sec}$ where the "beating" appears once more. During the "beating" the wave amplitude reaches a maximum of .9 cm and a minimum of .4 cm. The beating is confined to the region between $f = 2.09 \text{ rad/sec}$ and 2.88 rad/sec . At $f = 2.88 \text{ rad/sec}$ a finite amplitude wave is set on with an amplitude reaching 1.3 cm, the largest

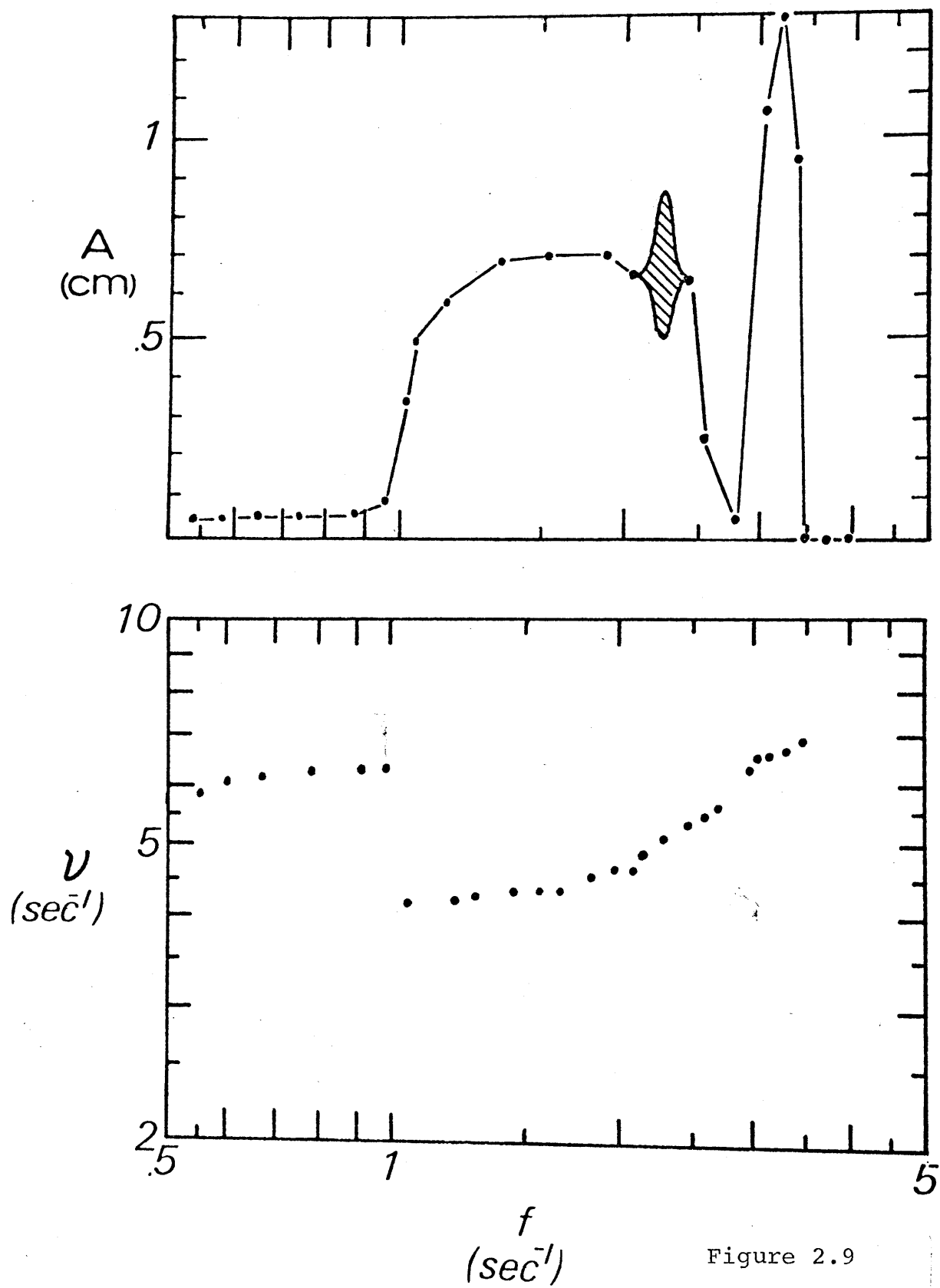


Figure 2.9

recorded. This finite amplitude persisted until $f = 3.5$ rad/sec where the wave disappeared for the range up to $f = 4.2$ rad/sec where the experiment was terminated.

Unlike experiment #3 in Section 2.7, the frequency range of this experiment breaks up clearly into four regions. These regions are (1) the region from $f = .5$ rad/sec to $f = 1.06$ rad/sec, (2) $f = 1.06$ rad/sec to $f = 2.09$ rad/sec, (3) $f = 2.09$ rad/sec to $f = 2.88$ rad/sec, and (4) $f = 2.88$ rad/sec to $f = 3.32$ rad/sec, where $v = 6.3$ rad/sec, $v = 4.2$ rad/sec, $v \propto f^{.71}$ and $v \propto f^{.47}$, respectively. The large break in slope between the last two regions lends credence to the frequency transition always paralleling the amplitude transition. If the region from 2.09 rad/sec to $f = 3.32$ rad/sec is taken as one region then the slope of v is $f^{.84}$. This result is a poor fit to the data and therefore the result is found that there are indeed a total of four regions.

In this last experiment it is found that there exist four distinct regions in both amplitude and frequency. These four regions pertain to the "microwave" behaviour, finite amplitude bore behaviour, "beat" type behavior and finite amplitude wave behaviour.

2.9 Experimental Conclusions

There exist four distinct regimes labelled here the microwave region, finite amplitude bore region, the beat region, and the finite amplitude wave region. These four regions correspond to a constant wave frequency for the first two types and

an f dependence for the last two types. Though all these types appeared in the last experiment, all four did not appear in the other three experiments. A summary of the results of the experiments are given in Table 1. The "beat" type behaviour did not occur in the small pump parameter range. The "microwave" occurred only for the large pump and large hole. The most important results to sum up are that the waves were for certain regions in each experiment independent of the table rotation rate and that in different regions they were dependent upon a function that behaved as approximately the square root of f . When smaller holes were used, i.e., less than 3.81 cm, no waves appeared whatsoever.

2.10 Lagrangian Tracer Results

Knowing the flow regime in the experiment helps to determine to what extent the wave influences the steady state thereby helping in formulating the problem. Figures 2.12-2.14 show the particle paths for experiments with a large exit hole (4.8 cm), large pump ($640 \text{ cm}^3/\text{sec}$) and various rotation rates where a bore appeared. The most obvious characteristic is that of the unsteady behaviour of the particles. A number of different particle traces appear in each of the figures. The long spiral track follows the path that is predicted by the steady state theory. There also occur in these figures flows that are almost entirely radially inward. These behave almost as if there were no rotation present. Two very anomalous cases of flow reversal appear in figure 2.11. There occurs

Table 1

	"Microwave"	Bore	"Beat" Wave	f Dependent Wave
SP, 3.8 cm	-	f = 0.44 v = 3.3	-	f = 1.38 v \propto f ^{.59}
SP, 4.8 cm	-	f = 0.73 v = 3.4	-	f = 1.72 v \propto f ^{.59}
LP, 3.8 cm	-	f = 0.46 v = 4.0	f = 1.33 v \propto f ^{.42}	f = 2.01 v \propto f ^{.52}
LP, 4.8 cm	f = 0.56 v = 6.2	f = 1.06 v = 4.2	f = 2.09 v \propto f ^{.71}	f = 2.88 v \propto f ^{.47}

SP = Small Pump, 400 cm³/sec

LP = Large Pump, 640 cm³/sec

f = twice the table rotation rate [rad/sec]

v = wave angular frequency [rad/sec]

$f = .89$

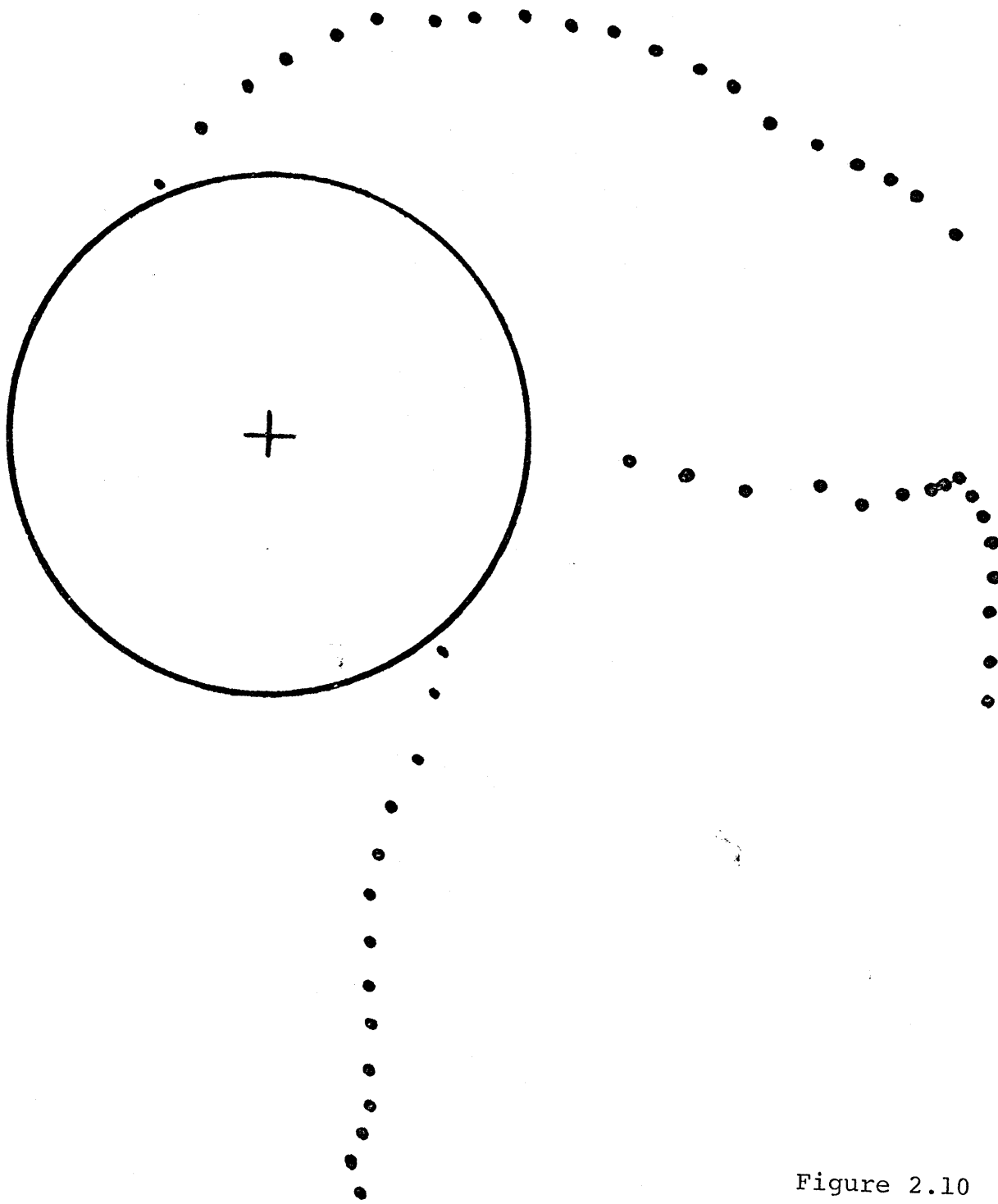


Figure 2.10

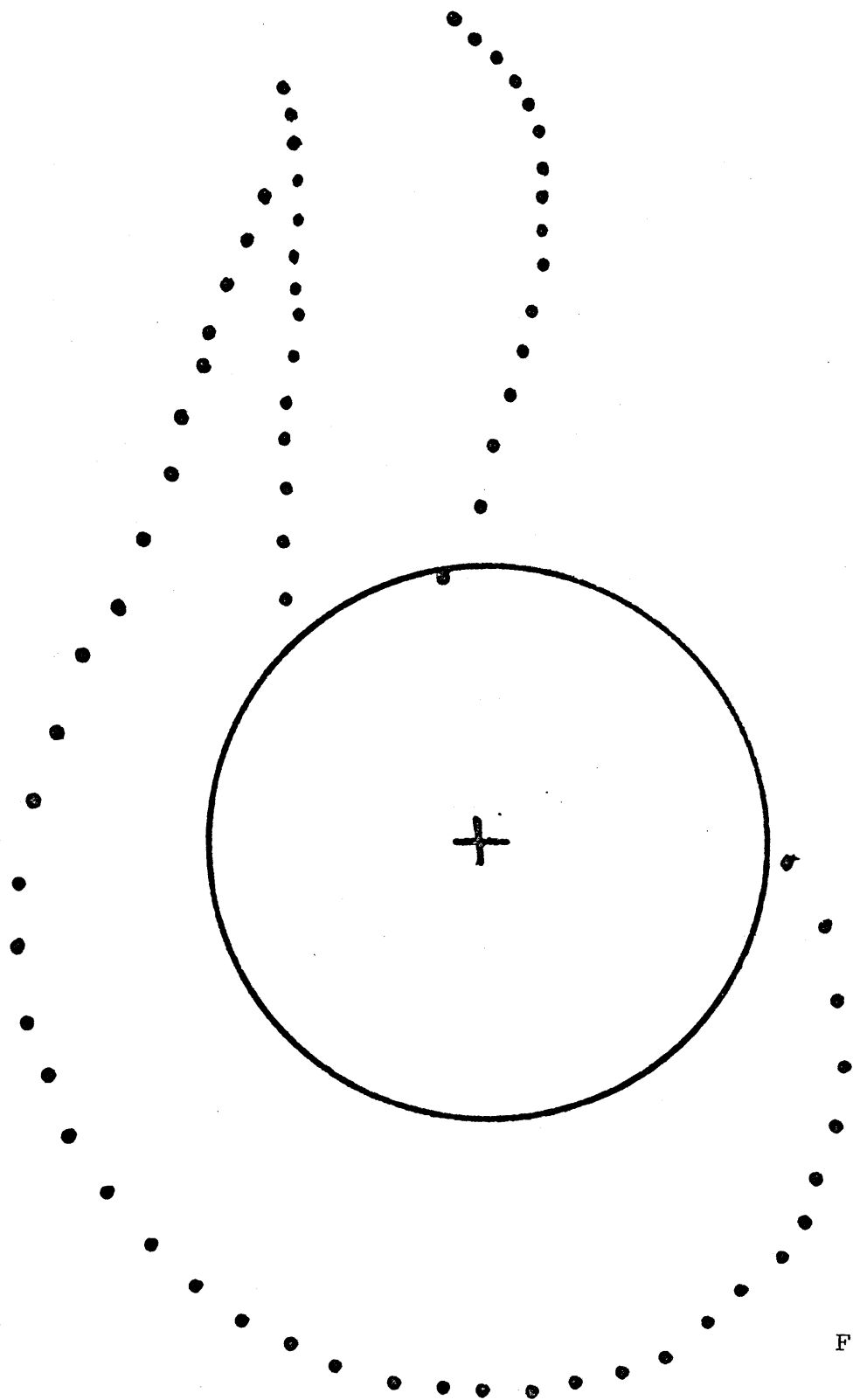


Figure 2.11

$$f = 1.33$$

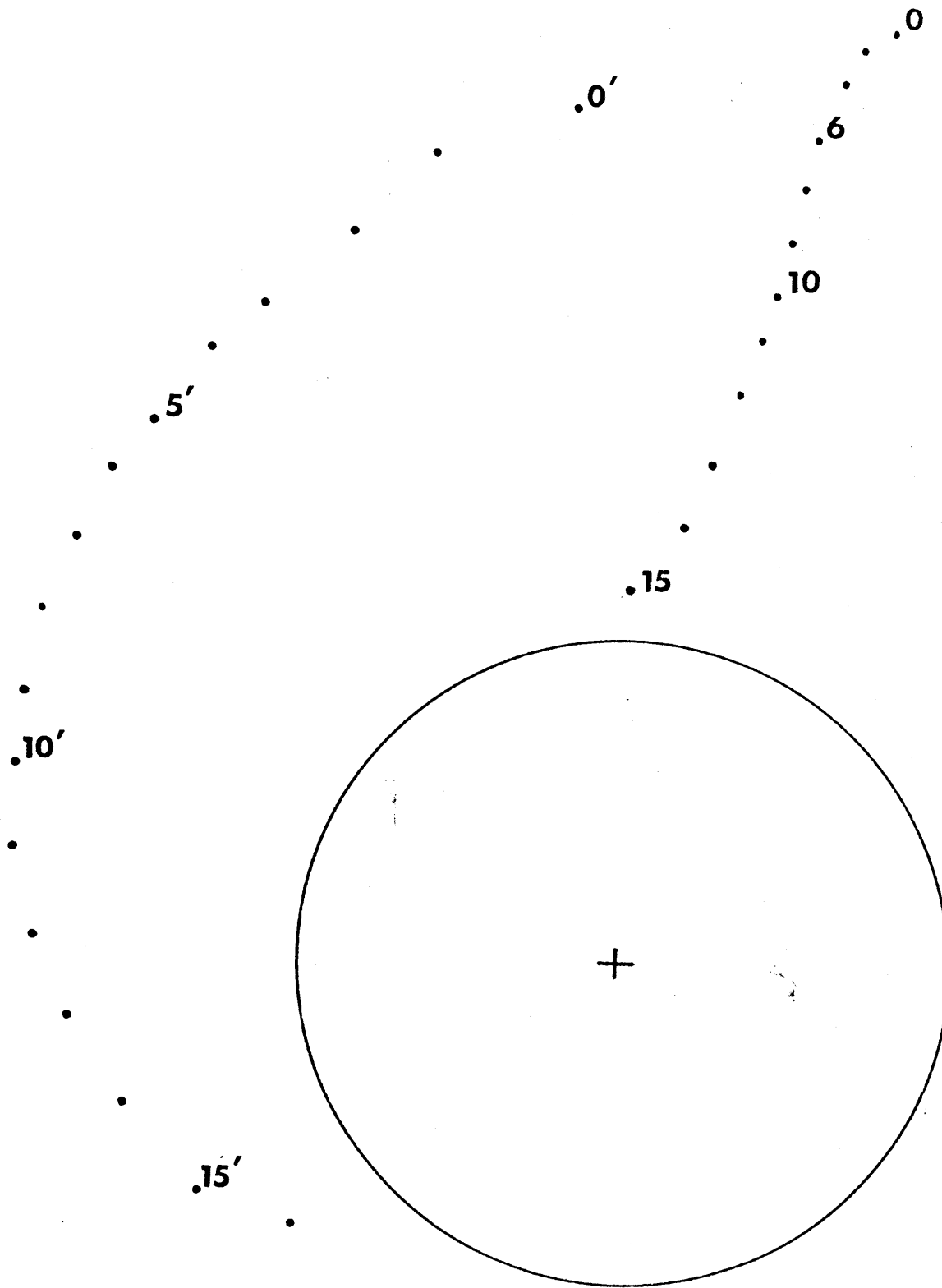


Figure 2.12

$f = 1.5$

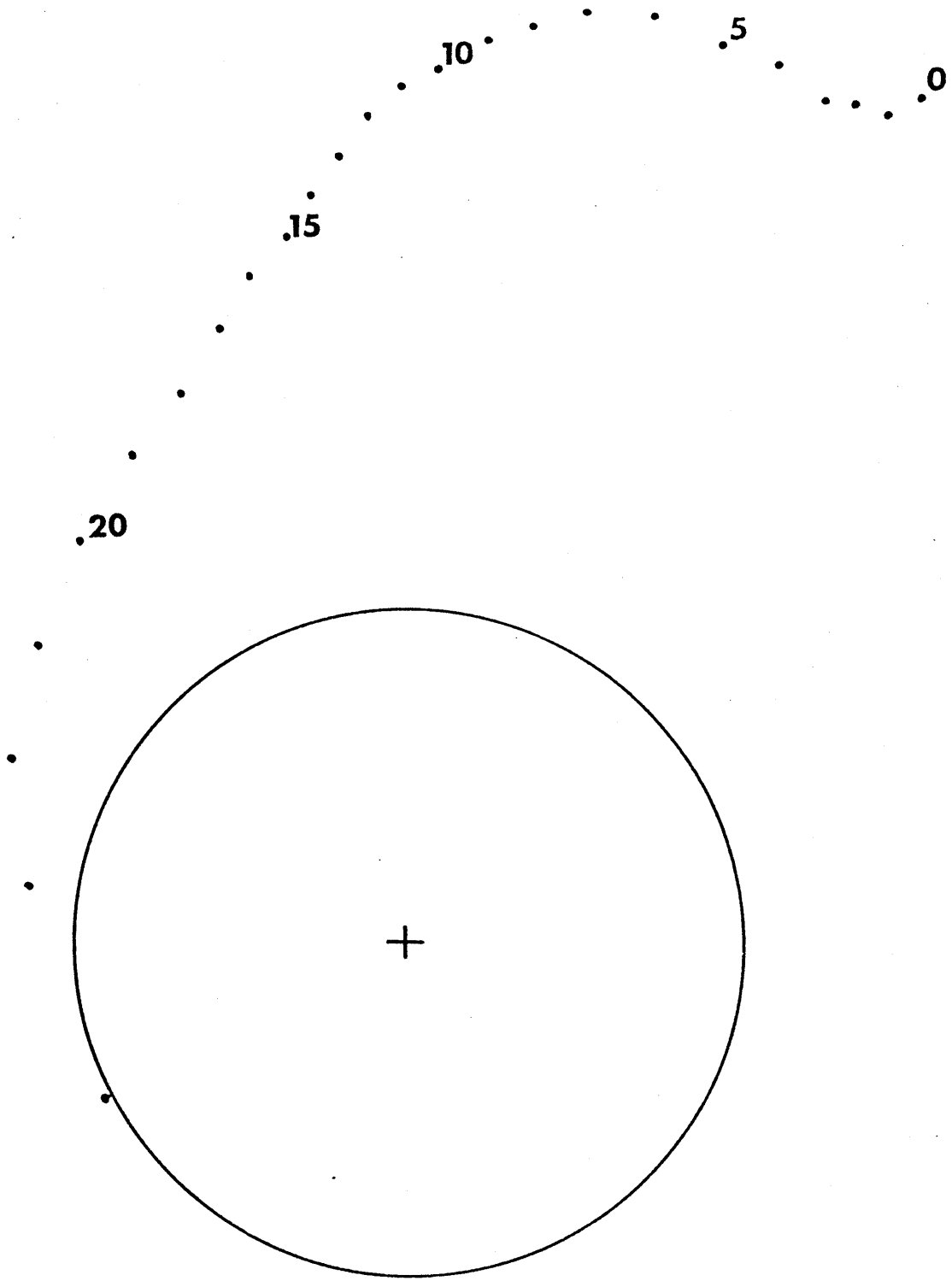


Figure 2.13

$$f = 2.25$$

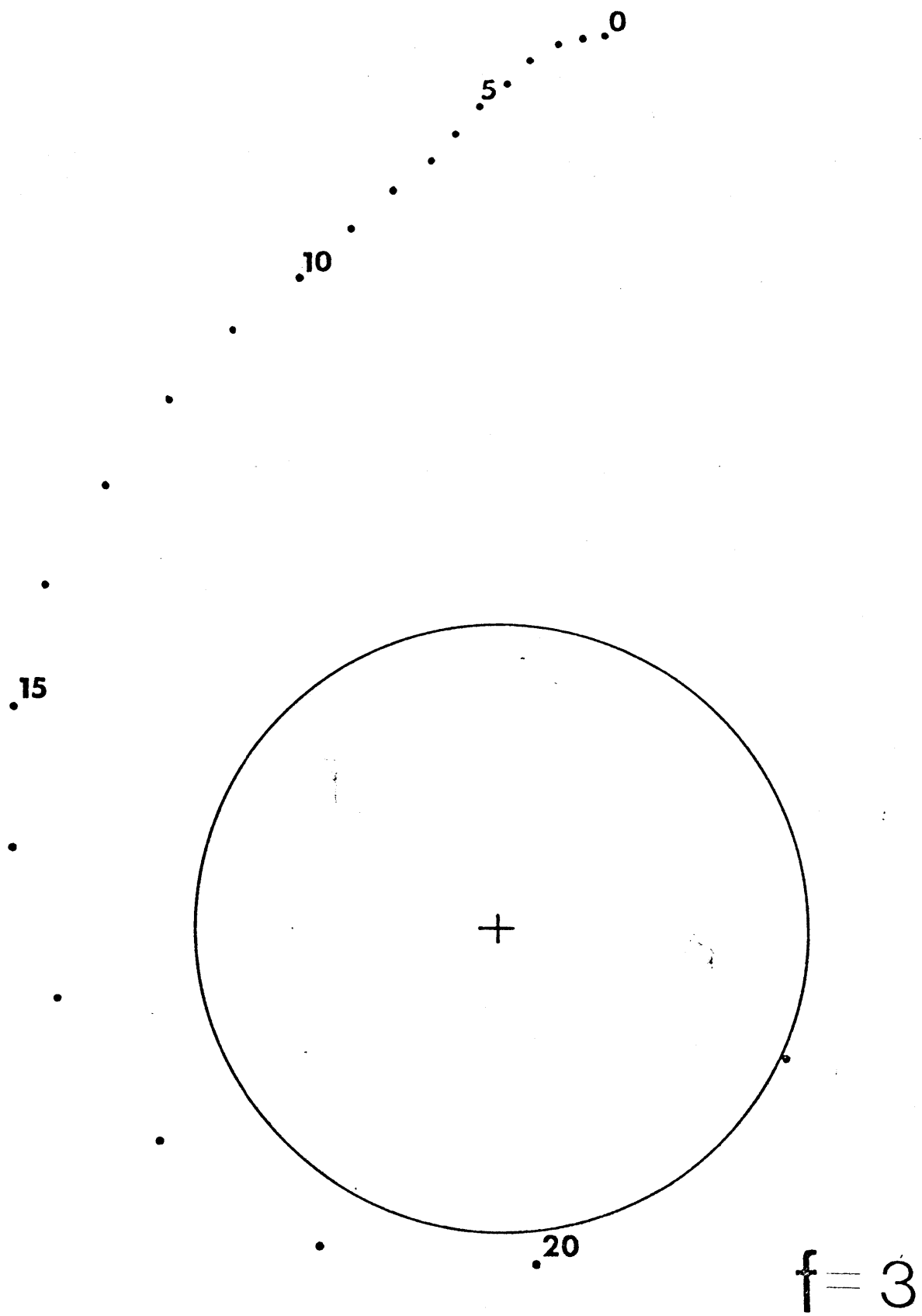


Figure 2.14

in the spiral case of this figure a flow that has a component that is radially outward for part of the spiral. There also occurs in the radially inward flow a reversal in the azimuthal direction.

Figures 2.13 and 2.14 correspond more to the case when there was a wave present rather than a bore. As in figure 2.11 so also in figure 2.13 there appears a region where the flow is radially outward. Figure 2.14 is a case where the wave is of small amplitude and the result is that the mean flow dominates the flow regime. From these figures one may conclude that there exists both radial and azimuthal reversals in velocity. This is especially true at the lower rotation rates when fluid depth is equal to the wave amplitude. As the rotation rate increases the effect of the wave decreases and just the mean flow dominates.

2.11 Stratified Experiment

The stratified experiment shows only qualitatively what might be the stratified analogue of the experiment described above. After the withdrawal pipe was turned on and the gyre fully developed there appeared to be a wobbling of the gyre about the pipe. A wisp of this may be seen in figure 2.15. We can only suggest that this might be the instability manifested as a wave traveling in a prograde sense on this critical flow.

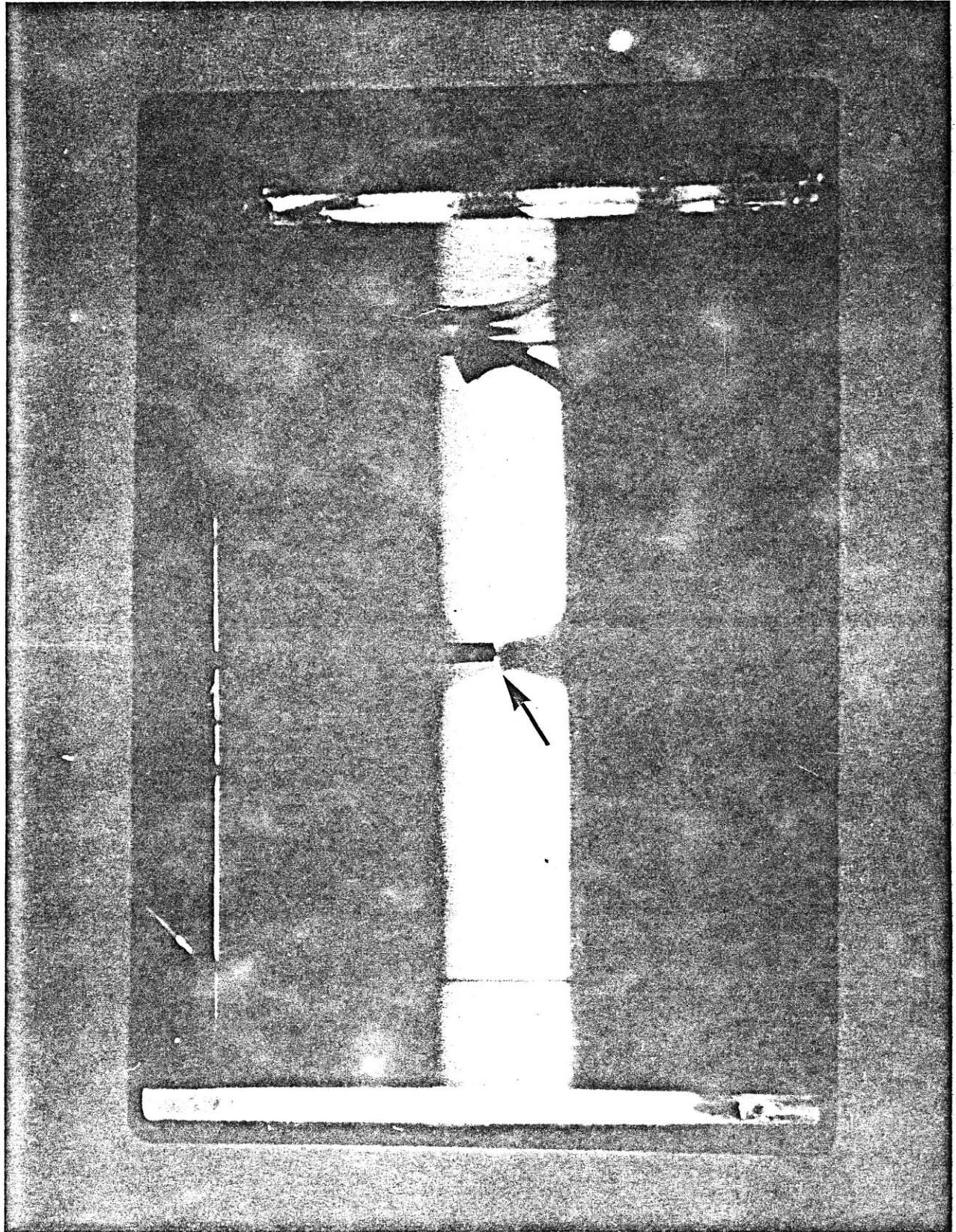


Figure 2.15

3.0 THEORY

3.1 Steady State Problem

The steady state emptying problem was solved analytically by Whitehead and Porter (1976). The time independent, inviscid, vertically integrated Navier-Stokes equations in polar coordinates were used. Axisymmetry was assumed. The independent variable is r , the radius from the axis of rotation. The dependent variables were u , the radial velocity, v the azimuthal velocity, and h , the height of the fluid. The gravitational acceleration is represented by the symbol g . The equations of motion then become

$$u \frac{\partial u}{\partial r} - \frac{v^2}{r} - fv = -g \frac{\partial}{\partial r} \left(h - \frac{f^2 r^2}{8g} \right) \quad (3.a)$$

and

$$u \left(\frac{\partial v}{\partial r} + \frac{v}{r} + f \right) = 0, \quad (3.b)$$

the radial momentum equation and the azimuthal momentum equation, respectively. The continuity equation is then

$$\frac{d}{dr} (r u h) = 0. \quad (3.c)$$

These equations are solved by ascertaining that the fluid is flowing always radially inward or outward, i.e., u is never zero. If u does not equal zero, then the equation in parenthesis in 3.b must equal zero, and a solution for v is obtained. The solution of the differential equation in (3.b) is

$$v(r) = \frac{c}{r} - \frac{fr}{2}. \quad (3.d)$$

The constant, c , in (3.d) may be determined from the boundary condition $v(r_1) = 0$, where r_1 is the radius of the diffuser. The statement that u is not equal to zero is analogous to the statement made in Whitehead, Leetmaa, and Knox (1973), that says the potential vorticity is equal to zero. The solution for v is substituted into equation (3.a) and with the use of the continuity equation (3.c) an algebraic equation in h is obtained,

$$gh^3 - gHh^2 + \frac{Q^2}{8\pi^2 r^2} = 0. \quad (3.e)$$

Where

$$H = h_1 + \frac{u_1^2}{2g} + \frac{f^2 r_1^2}{8g} - \frac{f^2 r_1^2}{8g} \frac{r_1^2}{r^2}, \quad (3.f)$$

Q is the flux of fluid through the pump and the subscript 1 refers to values at the diffuser wall.

This cubic in h may then be algebraically solved to obtain solutions of h and u . Equation (3.e) is of the same form as is the equation for inertial withdrawal of a non-rotating fluid from a cylindrical container except that the form of H is different. A plot of (3.e) in solution space shows that the solution cannot extend to all values of r . There exists a point where r is an extremum, i.e., $\frac{\partial r}{\partial h} = 0$. This defines the critical point in the flow where the change is made between sub- and super-criticality. With the boundary conditions given, the solutions of $u(r)$, $v(r)$, and $h(r)$ are uniquely determined.

There does exist a region of parameters in which the Ekman layer is capable of emptying the fluid faster than critical

withdrawal is. If it is assumed that all the transport is in the Ekman layer, then

$$Q = 2\pi v \delta, \quad (3.g)$$

where

$$\delta = (\mu/2f)^{1/2}. \quad (3.h)$$

The symbol μ is the viscosity. Q is the flux and is constant. If geostrophy is assumed, v , of equation (3.g) may be used and the geostrophic equation can be integrated to obtain h in the form

$$h_1 = \frac{Q}{\sqrt{2\mu} \pi g} \ln\left(\frac{r_1}{r_0}\right) f^{3/2} + \frac{Q^2 f}{4\pi^2 \mu} \left(\frac{1}{r_0^2} - \frac{1}{r_1^2}\right) + \frac{f^2 (r_1^2 - r_0^2)}{8g}. \quad (3.i)$$

This solution shows for the experimental parameter range the viscous boundary layer is capable of emptying the fluid faster than is the critical control, when the rotation rate is approximately $f = 6$ rad/sec. None of the experiments described so far in this paper have had parameters in that range of f .

An experiment was performed to test the theory by measuring the upstream depth and comparing it to theory, thereby verifying the depth averaging and inviscid assumptions. The results are in figure 3.1. This graph shows that for various pumping rates and rotation rates the data fall near the theoretical curve. At high rotation there is some discrepancy where the data points fall below the theoretical curves. This is due to the Ekman layer withdrawal dominating at high rotation rates. All the

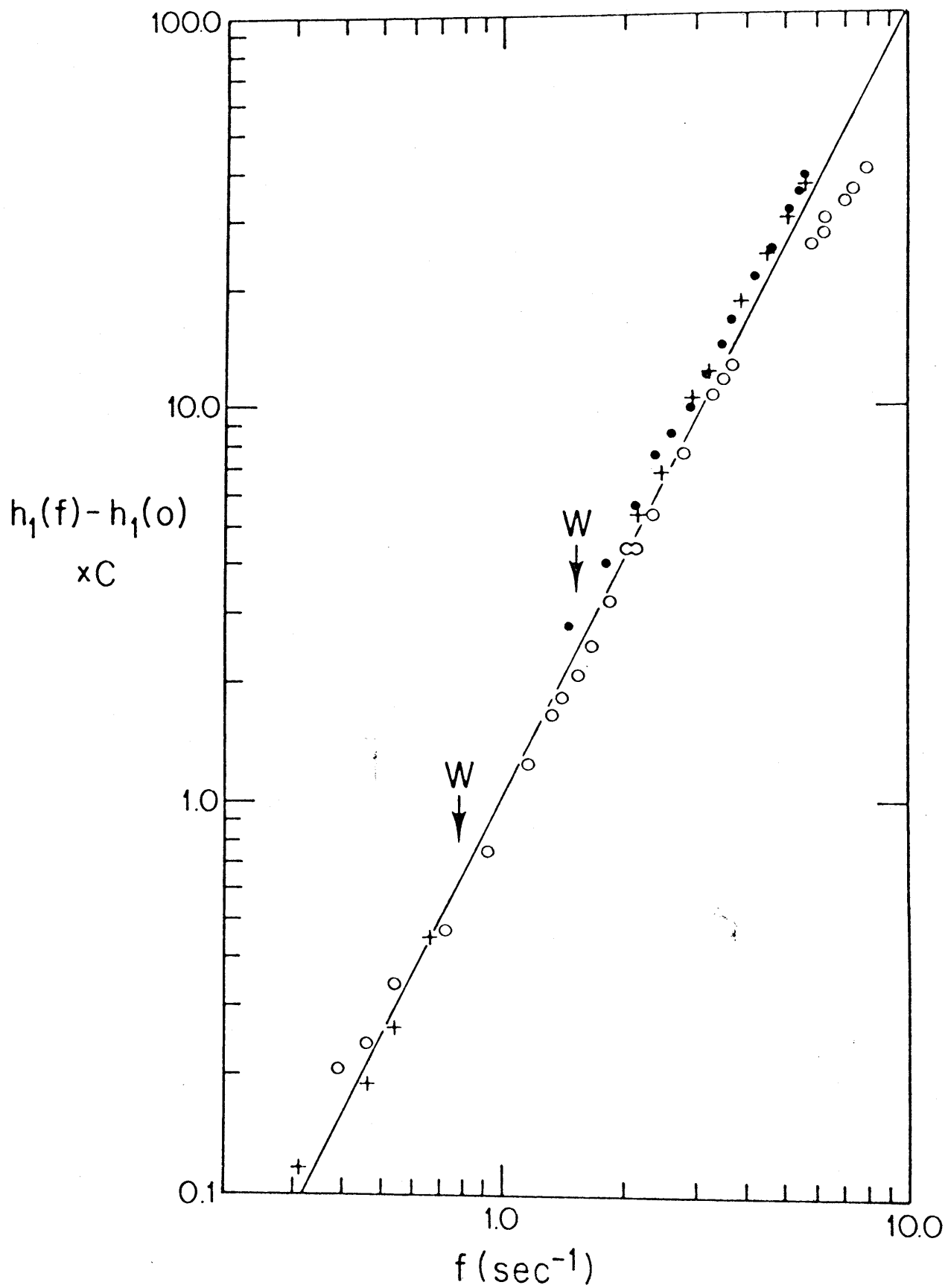


Figure 3.1

data were scaled by the factor C that takes into account not only the pumping rate but also the position of the probe used to measure the height of the upstream depth.

3.2 Dimensional Analysis

By use of dimensional analysis a time scale is obtained that is used to scale the full Navier-Stokes equations. The important parameters to be used, that completely determine the system, are r_0 the exit hole radius, r_1 the outside radius, g the gravitational acceleration, Ω the rotation rate of the table, and Q the flux of the fluid through the system. These parameters may be used to define three different time scales. These time scales are

$$\omega_1 = g r_0^2 / Q ,$$

$$\omega_2 = \sqrt{g/r_0} ,$$

(3.j)

and

$$\omega_3 = Q/r_0^3 .$$

If the transition frequencies, i.e., the frequency when the wave is onset and the frequency when the wave frequency becomes f dependent, are plotted as functions of r_0 and Q , then it can be shown that the scaling that most reduces the curves to a single graph is ω_1 . A scaling does not necessarily tell one about the physics involved, but it is a first step in ascertaining which terms in the full equations are important. With the scaling above the time scale is computed to be $\tau = .3$ sec for the large

pump and large hole and $\tau = .08$ sec for the small pump and large hole. With this time scale the Navier-Stokes equations are investigated.

3.3 Navier-Stokes Equations

With a time scale defined, the full time dependent Navier-Stokes equations can be scaled to discover which, if any, of the terms may be dropped to simplify the equations. The independent variables are t , the time, r , the radius measured from the axis of rotation, and θ , the azimuthal variable. The dependent variables are u , the radial velocity, v , the azimuthal velocity, and, h , the height of the fluid. The gravitational acceleration is denoted by the symbol g . The time dependent, inviscid, vertically integrated, Navier-Stokes equations then become

$$\frac{\partial \hat{h}}{\partial t} + \frac{1}{r} \frac{\partial ru\hat{h}}{\partial r} + \frac{1}{r} \frac{\partial v\hat{h}}{\partial \theta} = 0, \quad (3.k)$$

$$\frac{\partial u}{\partial t} + u \frac{\partial u}{\partial r} + \frac{v}{r} \frac{\partial u}{\partial \theta} - \frac{v^2}{r} - fv = -g \frac{\partial}{\partial r} \left(\hat{h} - \frac{f^2 r^2}{8g} \right) \quad (3.l)$$

and

$$\frac{\partial v}{\partial t} + u \frac{\partial v}{\partial r} + \frac{v}{r} \frac{\partial v}{\partial \theta} + \frac{uv}{r} + fu = -\frac{g}{r} \frac{\partial \hat{h}}{\partial \theta}. \quad (3.m)$$

A perturbation technique is used in equations (3.k)-(3.m) by re-defining the dependent variables as

$$\begin{aligned} \hat{h} &= h(r) + h'(r, \theta, t), \\ u &= u(r) + u'(r, \theta, t), \end{aligned} \quad (3.n)$$

and
$$v = v(r) + v'(r, \theta, t).$$

By substitution of the terms in (3.n) into the equations (3.k)-(3.m) a number of double terms appear that are of the forms pq , $p q'$, and $p'q'$. The double primed terms are assumed to be smaller than those of the other type and are dropped. The remaining terms are then scaled by the following factors,

$$\begin{aligned}\tilde{u} &= \frac{Q}{2\pi r_o H_o} u, & \tilde{u}' &= U_o u', \\ \tilde{v} &= \frac{f r_1^2}{2r_o} v, & \tilde{v}' &= V_o v', \\ \tilde{r} &= r_o r, & \tilde{t} &= \left(\frac{Q}{g r_o^2}\right) t,\end{aligned}$$

and

$$\tilde{h}' = h_o h'.$$

Dropping the tilde, the scaled equations are:

$$\frac{\partial u'}{\partial t} + B \left[u \frac{\partial u'}{\partial r} + u' \frac{\partial u}{\partial r} \right] + C \left[\frac{v}{r} \frac{\partial u'}{\partial \theta} - 2 \frac{V_o}{U_o} \frac{v v'}{r} - 2 \frac{r_o^2}{r_1^2} \frac{V_o}{U_o} v' \right] = -F \frac{\partial h'}{\partial r}, \quad (3.o)$$

$$\frac{\partial v'}{\partial t} + B \left[u \frac{\partial v'}{\partial r} + \frac{u v'}{r} \right] + C \left[\frac{v}{r} \frac{\partial v'}{\partial \theta} \right] = -F \frac{U_o}{V_o} \frac{1}{r} \frac{\partial h'}{\partial \theta}, \quad (3.p)$$

and

$$\frac{\partial h'}{\partial t} + B \left[\frac{1}{r} \frac{\partial r u h'}{\partial r} \right] + C \left[\frac{2}{r} \frac{\partial v h'}{\partial \theta} \right] = \frac{-F H_o}{h_o^2 g} \left[\frac{U_o}{r} \frac{\partial r u' h}{\partial r} + \frac{V_o}{r} \frac{\partial v' h}{\partial \theta} \right], \quad (3.q)$$

where

$$B = \frac{Q^2}{2\pi r_o^4 g} \frac{1}{H_o}, \quad C = \frac{Q r_1^2}{2r_o^4 g} f, \quad \text{and}$$

$$F = \frac{Q}{r_o^3} \frac{h_o}{U_o}.$$

If the parameters of the experiment are used to determine the values of the scaling terms, then the term denoted by an asterisk is the only term sufficiently small that it could be ignored. Unfortunately, this does not allow the equation to be simplified enough to obtain an analytical solution.

Since only one term can be dropped from our dimensional analysis of the problem, and that term does not simplify matters, it shall be kept in the analysis. The dimensional equations are reclaimed and a wave-like behaviour is assumed in which the terms $\frac{\partial p}{\partial t}$ and $\frac{\partial p}{\partial \theta}$ are replaced by $i\omega p'$ and imp' respectively. With this assumption the full equation is,

$$A \frac{\partial \tilde{U}'}{\partial r} = B \tilde{U}' , \quad (3.r)$$

where

$$A = \begin{bmatrix} u & 0 & g \\ 0 & u & 0 \\ h & 0 & u \end{bmatrix} ,$$

$$B = \begin{bmatrix} -i\omega - \frac{\partial u}{\partial r} - im \frac{v}{r} & \frac{2v}{r} + f & 0 \\ 0 & -i\omega - \frac{u}{r} - \frac{imv}{r} & -\frac{gim}{r} \\ -\frac{h}{r} - \frac{\partial h}{\partial r} & -\frac{\partial h}{\partial r} - \frac{imh}{r} & -i\omega - \frac{u}{r} - \frac{\partial u}{\partial r} \end{bmatrix} ,$$

and

$$\tilde{U}' = \begin{bmatrix} u' \\ v' \\ h' \end{bmatrix}$$

The point at which this set of equations is singular is found by taking the determinant of A. When the determinate of A

equals zero, then the equations are singular. $\text{Det } A = u(u^2 - gh) = 0$ when $u = 0$ or when $u = \sqrt{gh}$. The later statement is just that the Froude number is equal to one and this occurs only at the lip of the exit hole. On the other hand, $u = 0$ could happen as the flow reverses, as seen from the Lagrangian tracers, Section 2.10. The numerical solution of this set of simultaneous, first order, ordinary differential equations is beyond the scope of this investigation. If these equations were solved, then the point at which the instability occurs could most likely be found.

3.4 Wave Front

By purely kinematic considerations a set of equations may be derived that are able to test the formula for the wave speed. The wave speed is assumed to be that of the shallow water wave speed and therefore of the form \sqrt{gh} . The crest of the wave is defined by the function $s(r)$, where, $s(r) - \theta = 0$. The crest travels in the azimuthal direction at an angular velocity of v_r , where r is the distance from the axis of rotation. If the crest is viewed from the wave frame of reference, the picture developed is a stationary crest with the fluid flowing rapidly under the crest. The diagram in figure 3.3 shows that the wave is traveling in the \hat{n} direction and since it is stationary, it must be exactly balanced by the \hat{n} component of flow of the fluid underneath it.

This configuration may be stated mathematically as

$$\{-u(r)\hat{r} + (v(r) - v_r)\hat{\theta}\} \cdot \hat{n} = -\sqrt{gh} . \quad (3.s)$$

The normal vector to the wave crest is defined as

$$\begin{aligned}\hat{n} &= \frac{\nabla(S(r) - \theta)}{|\nabla(S(r) - \theta)|} \\ &= \frac{\frac{\partial S}{\partial r} \hat{r} - \frac{1}{r} \hat{\theta}}{\sqrt{\left(\frac{\partial S}{\partial r}\right)^2 + \frac{1}{r^2}}}\end{aligned}\quad (3.t)$$

By use of the definition of \hat{n} in equation (3.s) S' can be solved for in terms of u , v , and h , i.e.,

$$\frac{\partial S}{\partial r} = \frac{-u(v-vr) \pm \sqrt{(u^2 + (v-vr)^2 - gh)gh}}{r(u^2 - gh)} \quad (3.u)$$

This differential equation becomes singular when the Froude number is unity.

The analytical solution for the steady state formulation of v was used. The depth of the fluid, h , was approximated by using the Bernoulli head rather than the actually computed fluid depth, due to the algebraic complexity of h 's form and to the fact that the Bernoulli head is a good approximation to h . The solution of equation (3.u) was solved numerically by use of the Runge-Kutta method. As figure 3.4 shows, the solution follows the actual measured wave crest quite well, but the solution goes complex at $r = 6$ cm. The implications of this result are that the wave does travel at a speed near that of the shallow water wave speed. This formulation gives no information concerning the physics of the instability.

The result of the analysis above has actually little information in it due to the reversals in flow observed and the

nonlinearity of the wave. The flow reversals from figures 2.11 and 2.13 show that there do exist points where u and v are equal to zero giving rise to a complex equation in (3.u). This complex behaviour throws doubt on the validity of the formulation of the problem. Another important point is shown by Fourier decomposing the wave. Figure 3.2 shows the decomposition of the bore and triangular type wave. The bore shows there is a lot of information at frequencies that are higher than just that of the first mode. This underlines the nonlinearity of the system.

The theoretical section of this paper showed that various approaches began to allow some information to be gleaned, but that the next step should be the numerical solution of the full equations. A dimensional analysis showed that the most probable time scaling for the equations was Q/gr_0^2 . Using this in the linearized perturbation equations showed that the equations could not be easily converted to a tractable analytic form. They did show that the equations were singular when $u = 0$ and when the Froude number was unity. The solution of those equations would help to ascertain what terms are responsible for the instability. The kinematic approach allowed only the weak statement that the wave propagated near the speed of the shallow water wave. But the dubious result was weakened by the fact of flow reversals.

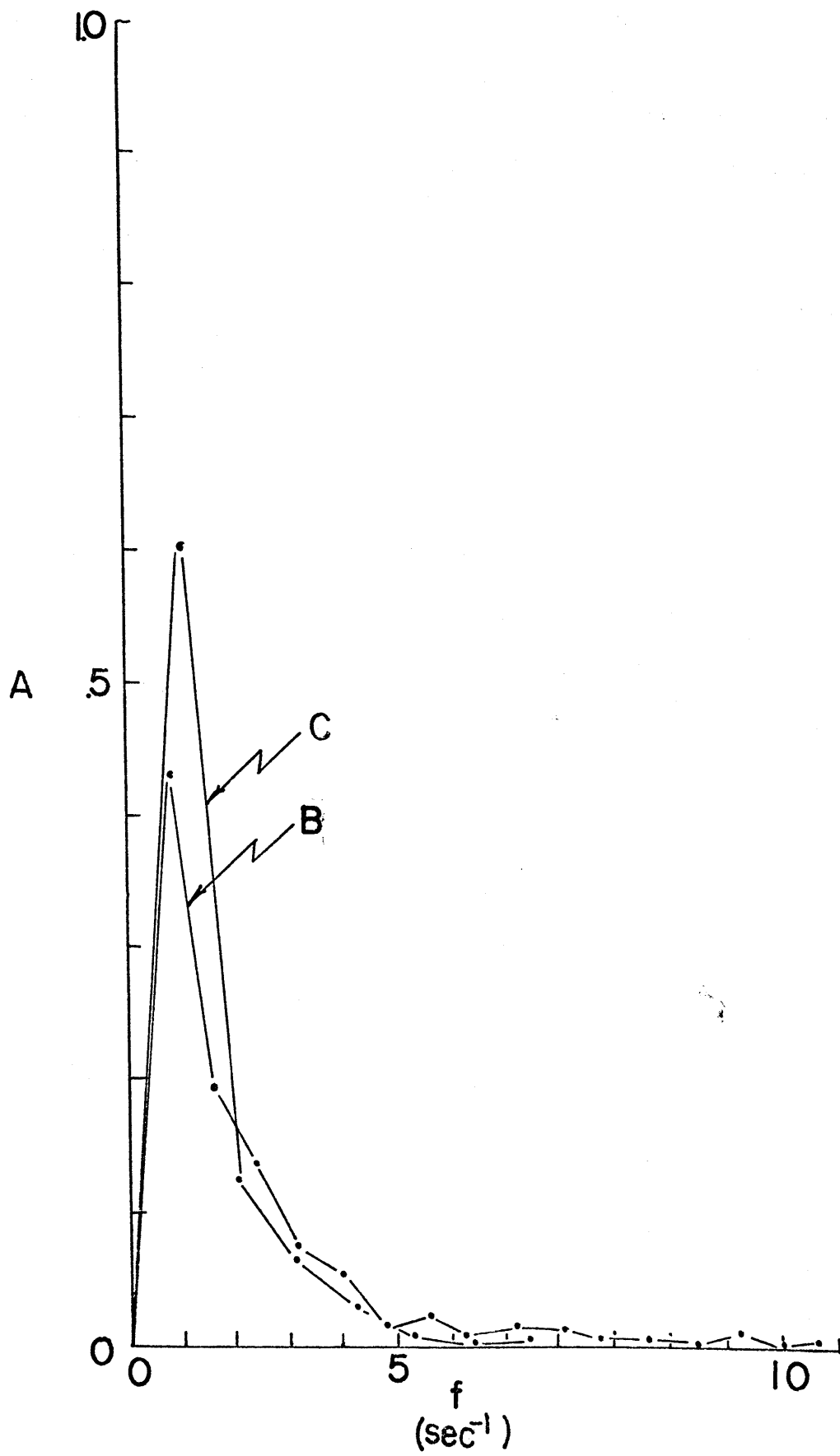


Figure 3.2

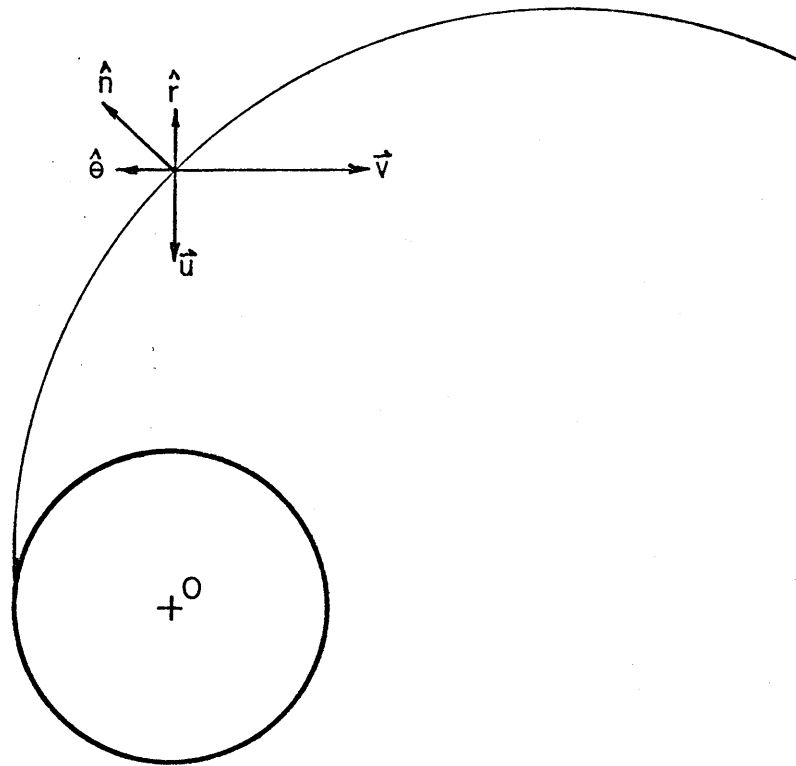


Figure 3.3

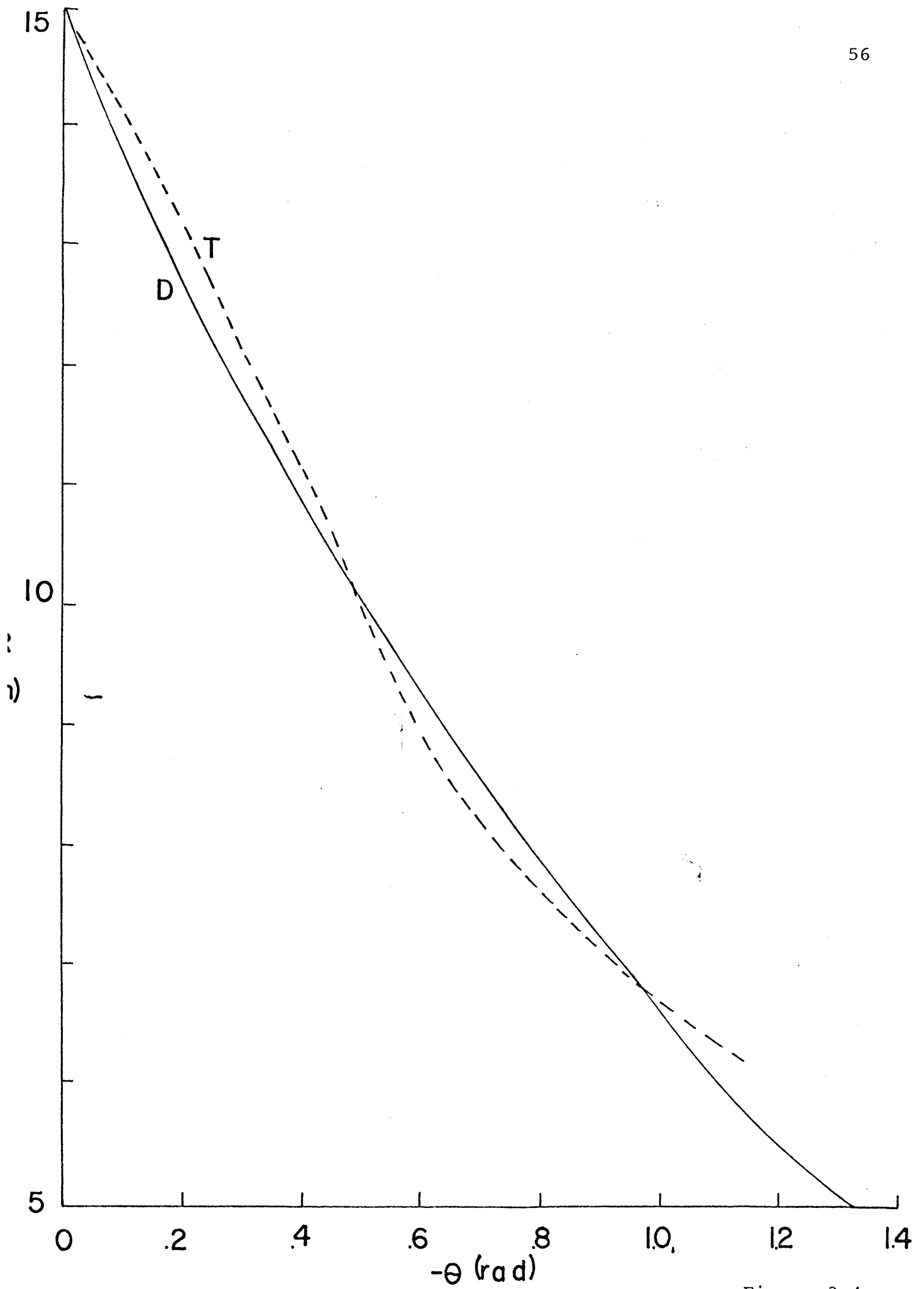


Figure 3.4

4.0 SUMMARY

When a rotating axisymmetric container is emptied through a concentric hole in the bottom, an instability manifested as an azimuthally travelling wave is observed. The wave has a crest that stretches from the inner exit hole to the outside wall and travels in the prograde sense. As a function solely of rotation rate the wave goes through a number of transitions in both amplitude and frequency when the exit hole size and pumping rate are fixed.

The experiments were conducted with different hole sizes and pumping rates. As a function of rotation rate there appeared to be three and maybe four unique regimes that the wave possessed. These four regions are (1) the "microwave" region, (2) the finite amplitude bore region, (3) the region that appears as the beating between two waves of different frequencies, and (4) the finite amplitude wave region. Regions two and four listed above are the only regions that were common to each experiment. The waves are independent of table rotation for the first two type waves and are dependent (as approximately the square root of f) on the table rotation rate for the last two types listed above. These are the general results, the exact parameters and their experimental results are summed up in Table 1.

Physically what one is seeing is probably an instability caused by the feedback mechanism at the exit hole. How deep the water is at the lip determines how fast it empties and how fast it empties influences how deep it is upstream. Results

were found using kinematics that showed that the wave traveled at approximately the shallow water wave speed, i.e., \sqrt{gh} . A perturbation analysis was also carried out that showed the equations were singular when $u = 0$ or when the Froude number equalled unity. The condition of the Froude number being unity occurred at the lip. The solutions of these equations will most probably lead to the calculation of when the instability is onset.

The interest in this problem lies not only in it being an apparent instability in a critical flow problem but also in its possible applications to geophysical and engineering problems. The geophysical problem is that concerned with flow over oceanic sills. All the major ocean basins are connected through a number of sills and deep ocean straits. It is conceivable that the same mechanism that is at play in the emptying of this container could also be at work in the oceanic deep sills. This may be part of the explanation for the "bursting" observed in the current meter records from deep ocean sills. An example of this is the Windward passage sill in the Caribbean Sea. Current meter data from there shows bursts of large quantities of water out of the basin (Stalcup and Metcalf, private communication).

Two engineering problems where this instability might be of interest is in the operation of ocean thermal energy plants (OTEC) and in the emptying of fuel tanks on rockets. In the case of OTEC, where large quantities of water are drawn up from below the thermocline, the question is raised of not only how

important the earth's rotation is in the formulation of the steady state case, but also of whether this instability could be onset, thereby decreasing the plant's efficiency. In the case of rocket tanks emptying, it might be that the fluid being emptied had been given a spin and as it is withdrawn it reaches the stage where a bore is onset. This bore may impart an undesirable momentum to the craft.

In summary, an instability was observed that had a number of different transitions in wave amplitude and wave frequency as a function of rotation rate. Applications of this phenomenon can be made to geophysical and engineering problems as well as the investigation of how fluids are critically withdrawn.

APPENDIX A

The errors in measurements presented in the paper are good to within the last significant digit shown. The actual errors for the measurements are presented in this appendix.

The density of fluid that was measured in the stratified experiment was accomplished by measuring the fluid's index of refraction. This method yielded results that were accurate to within $.0005 \text{ gm/cm}^3$.

The pumping rates were measured under various conditions and found to yield results that were accurate to about 5%. The method used to obtain these measurements was to time how long it took for the basin to fill once the exit hole was blocked. In this manner the pumping rate could be measured for various heads. The resulting flow rates were $640 \pm 30 \text{ cm}^3/\text{sec}$ for the large pump and $400 \pm 34 \text{ cm}^3/\text{sec}$ for the small pump.

The table frequency measurements were found to be accurate to within $\pm .5\%$. The magnetic switch on the table and the recorded record of table rotation on the strip chart were accurate enough that the only errors in measurement were in reading the results off the chart. This error was reduced to less than $.5\%$ by the use of a measuring device accurate to $.05 \text{ mm}$.

The frequency of the wave was found to have a measured error of less than 1% . The transducer used had a response of approximately $.004 \text{ sec}$ and the chart recorder's response was similarly small, such that these effects were not important in the measurement. Thus the only error of importance was in

measuring the record off the strip chart. This proved to be accurate to less than 1%.

The amplitude of the wave was measured by use of a ruler and an error of 10% was assumed. The measured values were accurate to within 1% but the actual time variation in wave amplitude varied over 10% of the average. The actual variation in amplitude is thus the chief factor in the error.

The computation of the slopes of the lines in figures 2.6-2.9 were accomplished by a least squares fit of the data. The correlation coefficient was, in the worst case, .97. For the sample size tank this is a 4% error leading to an indeterminacy in the slope of approximately ± 0.03 .

APPENDIX B

The computation of the wave frequency was corrected for Doppler shifting (see page 23). This Appendix lists the data that was plotted up in figures 2.6-2.9. Though the Doppler shifting correction changed the values some, the salient features of the wave frequency were still prominent. The region of ν independent of f and the breaks in slope are still observable in the uncorrected data.

DATA EXPERIMENT #1
(Small Pump, 3.8 cm Hole)

f (rad/sec)	v_m (rad/sec)	v (rad/sec)
0.44	3.22	3.15
0.51	3.36	3.27
0.60	3.40	3.30
0.70	3.41	3.30
0.77	3.41	3.29
0.86	3.43	3.29
0.94	3.47	3.31
1.02	3.55	3.38
1.12	3.63	3.44
1.38	5.06	4.84
1.44	5.09	4.86
1.56	5.32	5.06
1.64	5.49	5.22
1.69	5.43	5.15
1.83	5.72	5.42
1.90	5.94	5.63
1.93	6.03	5.71
2.09	6.16	5.82
2.13	6.42	6.06
2.22	6.45	6.08
2.36	6.72	6.33
2.39	6.90	6.51
2.47	6.90	6.49
2.60	7.20	6.78
2.69	7.20	6.76
2.80	7.36	6.90
2.88	7.60	7.12
3.04	8.06	7.56
3.13	8.18	7.67
3.22	8.40	7.87
3.29	8.31	7.77
3.43	8.40	7.83
3.51	8.67	8.09
3.63	8.77	8.17
3.76	9.67	9.05

DATA EXPERIMENT #2
(Small Pump, 4.8 cm Hole)

f (rad/sec)	v_m (rad/sec)	v (rad/sec)
0.73	3.36	3.24
0.81	3.43	3.30
0.87	3.51	3.36
0.96	3.63	3.47
1.03	3.55	3.38
1.11	3.59	3.40
1.18	3.63	3.43
1.28	3.63	3.42
1.36	3.67	3.44
1.48	3.72	3.48
1.59	3.76	3.50
1.64	3.80	3.53
1.72	4.23	3.95
1.83	4.43	4.13
1.90	4.48	4.17
2.01	4.73	4.40
2.05	4.99	4.65
2.13	5.15	4.80
2.26	5.32	4.95
2.26	5.32	4.95
2.39	5.37	4.98
2.45	5.60	5.20
2.56	5.72	5.30
2.63	5.85	5.42
2.76	6.03	5.58
2.82	6.03	5.57
2.92	6.23	5.74
3.00	6.51	6.02
3.13	6.62	6.10
3.33	6.79	6.24
3.38	6.99	6.43
3.47	7.03	6.45
3.55	7.36	6.77
3.63	7.28	6.68
3.85	7.76	7.12
3.94	7.72	7.07
4.04	7.82	7.16
4.20	8.28	7.58

DATA EXPERIMENT #3
(Large Pump, 3.8 cm Hole)

f (rad/sec)	v_m (rad/sec)	v (rad/sec)
0.46	3.80	3.72
0.52	4.09	4.01
0.64	4.18	4.08
0.73	4.18	4.06
0.86	4.43	4.29
0.99	4.43	4.27
1.10	4.43	4.25
1.22	4.43	4.23
1.27	4.43	4.22
1.28	4.68	4.47
1.33	4.68	4.46
1.40	4.94	4.70
1.48	4.94	4.69
1.56	5.09	4.84
1.77	6.29	6.00
1.83	6.36	6.06
1.85	6.38	6.08
2.01	6.65	6.32
2.05	6.86	6.53
2.26	7.06	6.68
2.36	7.36	6.97
2.47	7.60	7.19
2.59	7.60	7.17
2.76	8.10	7.64
2.84	8.10	7.63
2.96	8.10	7.61
3.13	8.64	8.13

DATA EXPERIMENT #4
(Large Pump, 4.8 cm Hole)

f (rad/sec)	v_m (rad/sec)	v (rad/sec)
0.56	5.98	5.88
0.60	6.19	6.09
0.66	6.23	6.12
0.78	6.43	6.30
0.92	6.51	6.36
0.98	6.51	6.35
1.06	4.43	4.26
1.21	4.46	4.26
1.30	4.53	4.31
1.46	4.63	4.39
1.56	4.63	4.37
1.69	4.63	4.35
1.85	4.89	4.58
1.97	4.94	4.61
2.09	4.99	4.64
2.17	5.32	4.96
2.26	5.43	5.05
2.47	5.78	5.37
2.59	5.85	5.42
2.66	6.10	5.66
2.66	6.45	6.01
2.88	6.86	6.39
3.00	7.06	6.56
3.13	7.09	6.57
3.26	7.28	6.74
3.32	7.44	6.89

REFERENCES

Anderson, J. and J. Anderson, Jr., 1966.

Thermal Power from Sea Water. Mech. Eng. 88, 41-46.

Chisnell, R. F., 1966.

Outflow from a circular cylinder under the action of Coriolis force. Tellus XVIII, 77-78.

Sambuco, E. and J. Whitehead, 1976.

Hydraulic control by a wide weir in a rotating fluid. JFM, Vol. 73, pt. 3, 521-528.

Whitehead, J., A. Leetmaa, and R. Knox (1974).

Rotating hydraulics of strait and sill flows. Geophysical Fluid Dynamics, Vol. 6, 101-125.

Whitehead, J. A. and D. L. Porter (1976).

Axisymmetric critical withdrawal of a rotating fluid. Journal of Fluid Mechanics (In submission).

Zener, Clarence (1973).

Solar Sea Power, Physics Today (January), 48-53.

Biography

Name: DAVID LARSEN PORTER
 Date of Birth: 8th September 1951
 Place of Birth: Washington, D. C.

EDUCATION

Walter Johnson Senior High School, Bethesda, Maryland; 1969
 University of Maryland; 1973
 Degree: B.S.
 Major: Physics
 Minor: Mathematics
 Massachusetts Institute of Technology-Woods Hole Oceanographic
 Institution; 1976
 Degree: M.S.
 Major: Physical Oceanography

HONORS

High School: Honor Roll; Member National Honor Society
 University of Maryland: President of Sigma Pi Sigma;
 Departmental Honors; Honors with High Honors in Physics
 Massachusetts Institute of Technology-Woods Hole Oceanographic
 Institution: Associate Member MIT Chapter of Sigma Xi.

PUBLICATIONS

- "Spectral Characteristics of Internal Waves near the Väisälä
 Frequency," Desaubies, Yves and Porter, David, 55th
 Annual Meeting of the American Geophysical Union,
 April 8-12, 1974.
- "Geostrophic Calculations for the Alboran Sea," May, P. and
 Porter, D., Transactions of the American Geophysical Union,
 Vol. 56, No. 6, June 1975.
- "A Note on Eastern Boundary Currents in a Laboratory Analogue
 of the Ocean Circulation," Faller, A. and Porter, D.,
Tellus, XXVII, 1976, pp. 88-89.
- "Inertial Controls upon the Withdrawal of a Rotating Strati-
 fied Fluid," Whitehead, J. A. and Porter, D. L., Bulletin
 of the American Physical Society, Series II, Vol. 21,
 No. 10, November 1976.
- "Axisymmetric Critical Withdrawal of a Rotating Fluid,"
 Whitehead, J. A. and Porter, D. L., Journal of Fluid
 Mechanics (In submission).